2014

Analysis of multi-layered beam structures using spectral finite element method

Ahmet Unal

ANALYSIS OF MULTI-LAYERED BEAM STRUCTURES USING SPECTRAL FINITE ELEMENT METHOD

By

AHMET UNAL

A THESIS

Submitted in partial fulfillment of the requirements

for the degree of Master of Science in Engineering

in

The Department of Mechanical and Aerospace Engineering

to

The School of Graduate Studies

of

The University of Alabama in Huntsville

HUNTSVILLE, ALABAMA 2014

In presenting this thesis in partial fulfillment of the requirements for a master's degree from The University of Alabama in Huntsville, I agree that the Library of this University shall make it freely available for inspection. I further agree that permission for extensive copying for scholarly purposes may be granted by my advisor or, in his absence, by the Chair of the Department or the Dean of the School of Graduate Studies. It is also understood that due recognition shall be given to me and to The University of Alabama in Huntsville in any scholarly use which may be made of any material in this thesis.

Ahmet Unal

4/3/2014

(Date)

THESIS APPROVAL FORM

Submitted by Ahmet Unal in partial fulfillment of the requirements for the degree of Master of Science in Engineering in Mechanical Engineering and accepted on behalf of the Faculty of the School of Graduate Studies by the thesis committee.

We, the undersigned members of the Graduate Faculty of The University of Alabama in Huntsville, certify that we have advised and/or supervised the candidate on the work described in this thesis. We further certify that we have reviewed the thesis manuscript and approve it in partial fulfillment of the requirements for the degree of Master of Science in Engineering in Mechanical Engineering.

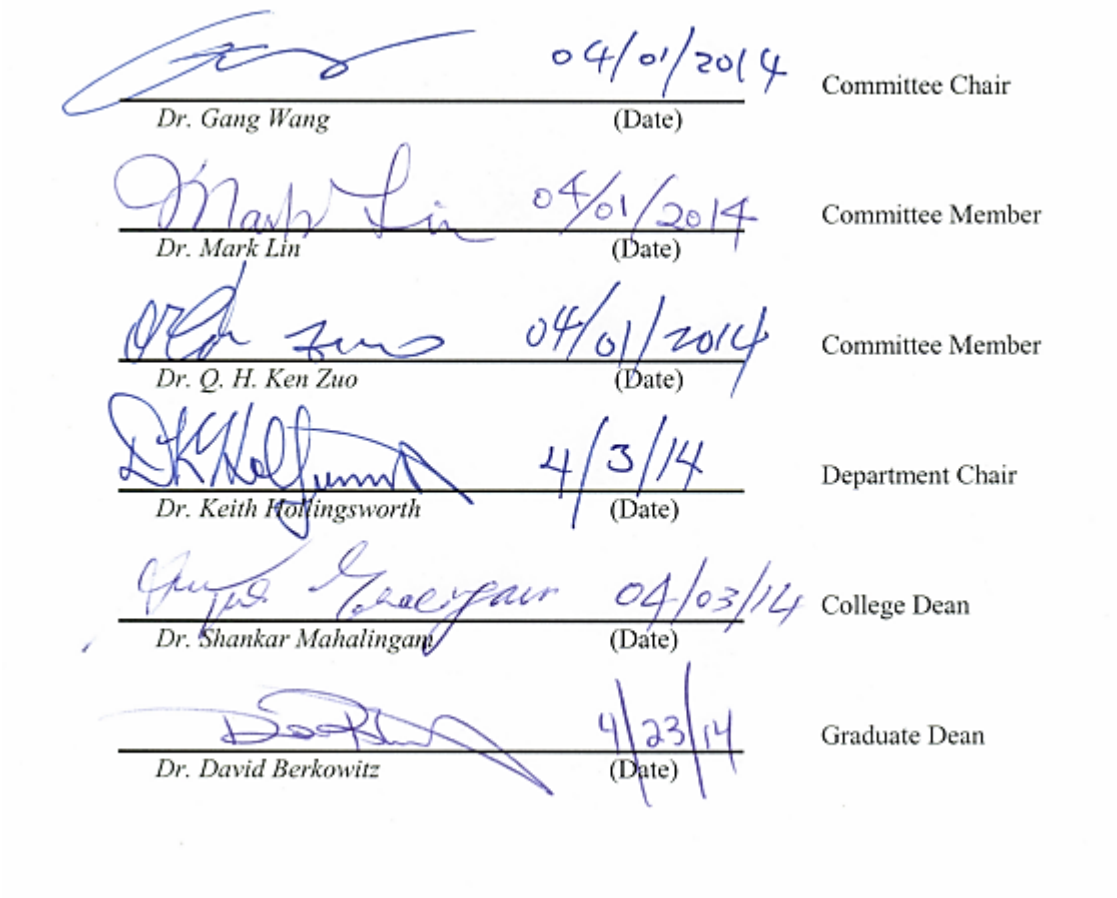

ABSTRACT
The School of Graduate Studies
The University of Alabama in Huntsville

Degree: Master of Science in Engineering College/Dept: Engineering / Mechanical and Aerospace Engineering

Name of Candidate: Ahmet Unal
Title: Analysis of Multi-Layer Beam Structures Using Spectral Finite Element Method

Multi-layered elastic structures are widely used in engineering applications due to their high strength, fatigue resistance and their ability to be tailored to meet different design requirements. Although they provide many benefits compared to their metallic counterparts, they are also susceptible to damage. In most cases, the damage detection in a multi-layered structure is challenging due to its complex structure and construction (e.g. delamination).

Lamb wave based structural health monitoring has been successfully implemented in metallic beam and plate structures. Damage location, amount and the extent can be determined by comparing baseline signatures of wave propagation in the structure. However, it is very challenging to characterize the dynamic behavior of a multi-layered structure and to extend wave based SHM to a multi-layered structure, in which the wave propagation characteristics must be well understood. Accurate prediction of high frequency wave response using conventional finite element method requires a large number of elements in the structural problem, resulting in computational effort and cost. A new high fidelity, efficient, and accurate model, and a solution approach are needed to capture the dynamic behavior of such multi-layered structures.

In this thesis, the spectral finite element model (SFEM) is developed to predict the dynamic behavior of a multi-layered beam structure. First, a higher order multi-layered beam model is

developed. For a beam that has *n* number of layers, each layer of the beam is idealized by a Timoshenko beam, in which shear deformation as well as rotational inertia are included. Mathematical model is developed based on this higher order theory, which is critical to capture high frequency response of the multi-layered beam structures. A set of fully coupled governing equations and associated boundary conditions are obtained by the application of Hamilton's principle. Secondly, semi-analytical solutions of these equations are determined in order to formulate the SFEM. The predictions of the SFEM are compared to the NASTRAN results and other data in literature. Fewer elements are required in the SFEM, compared to conventional finite element based approaches, which substantially benefits the ultrasonic frequency simulations. Finally, the newly developed SFEM is applied to the structural health monitoring demonstration in a multi-layered beam. Accurate wave propagation predictions in undamaged and damaged cases are captured.

Abstract Approval:

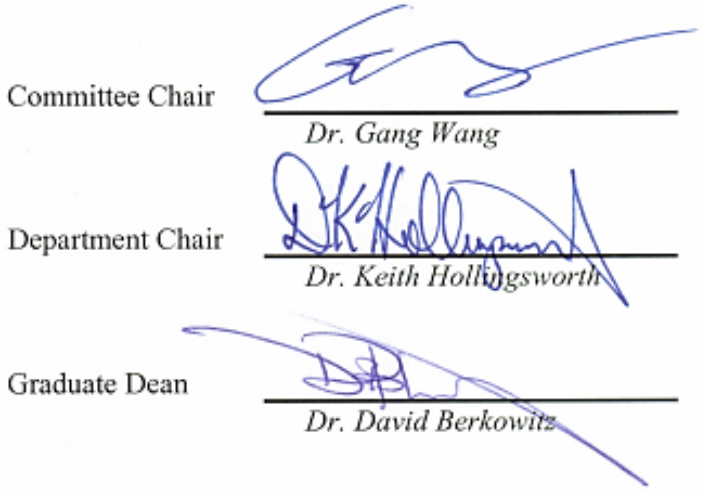

Acknowledgements

I would like to acknowledge all who helped me through my study. First, I would like to thank Dr. Gang Wang for guiding me, and for his encouragement that lead me doing this thesis. I am equally thankful to Dr. Ken Zuo and Dr. Mark Lin for being part of my thesis committee. I would also like to thank all the professors and teachers who have taught me, without them I would not have had the knowledge and encouragement to finish my thesis. Finally, I would like to thank my wife, for her unending patience and encouragement, and my two beautiful daughters for cheering me up whenever I needed.

TABLE OF CONTENTS

LIST OF FIGURES

FIGURE PAGE

LIST OF TABLES

LIST OF SYMBOLS

Symbol	Definition
n	Total Number of Layers
i	Layer Number
j	$\sqrt{-1}$
ω	Angular Frequency
t	Time
u	Axial Displacement
h	Height
b	Width
θ	Rotation
w	Transverse Displacement
$\bar{y}$	Local Coordinate Variable
ε	Strain
U	Strain Energy
E	Modulus of Elasticity
G	Shear Modulus of Elasticity
I	Moment of Inertia
A	Area
L	Length
T	Kinetic Energy
ρ	Density

m	Mass per Unit Length
W	Virtual Work
N	Axial Force
V	Shear Force
Z	State Vector

CHAPTER 1

INTRODUCTION

1.1 Background

Multi-layered structures have become increasingly popular in the construction of aerospace, mechanical, civil, marine, automotive and other high performance structures due to their high strength to weight ratio, excellent fatigue resistance, longer durability, and their ability to be tailored for specific applications as compared to their metallic counterparts. Many examples of multi-layered structures exist in the form of composite plate, beam and shell. Critical structural components made from these composite materials are often subject to significant multi-axial dynamic loads, which may considerably reduce their structural integrity, and result in a catastrophic failure. In addition, most of the time damage in a composite structure, like delamination, cannot be detected by visual inspection. To improve safety, reliability and operational life, it is essential to monitor the integrity of such structural systems. Many different types of advanced damage detection schemes provide a significant benefit in detection, identification and assessment of small defects in structures and provide tools for developing structural health monitoring (SHM) systems [1].

In recent years, particular attention has been given to the elastic wave propagation and wave based SHM has been successfully applied in the metallic beam/plate structures. Waves transmitted through the material interact with damage, resulting in the generation of reflecting waves, which can be analyzed to determine the damage type and/or extent in the structure. However, most composite structures being used today are composed of many different layers to

address different design requirements. In order to extend the wave based SHM to a multi-layered structure, the dynamics and wave propagation characteristics of such structure need to be understood. While conventional finite element method (CFEM) is a tool that has been extensively used in analyzing the dynamic characteristics of structures, it lacks the accuracy and efficiency in the analysis of wave propagation analysis since CFEM requires the element size to be 10-20 times smaller than the wavelength. In higher frequency analysis, the wavelength becomes smaller, driving the element size smaller, and resulting in a system composed of large number of elements. The accuracy of the solution may be increased by using higher number of elements, resulting in a very large problem size costing computation effort and time, which is a drawback of CFEM. Hence, alternatives to CFEM have been considered by many researchers.

1.2 Multi-Layered Beam Models

Classical laminated plate theory (CLPT) is one of the commonly used theories developed to analyze multi-layered structures [2]. However, it is an extension of the Kirchhoff (classical) plate theory, which assumes that plane sections remain plane during bending, to laminated composite plates, and neglects both transverse shear and transverse normal effects. In first order shear deformation theory, the relation is conducted to include shear deformation in each layer [2]. However, both theories neglect the warping effect. Krajcinovic [3] discovered that, for some short sandwich beams, neglecting warping effects can give 20% error in bending stress calculations. In the analysis, he presented a simple theory for a three layer sandwich beam, with each lamina following Bernoulli-Kirchhoff hypothesis, but the overall cross section was allowed to warp, because the rotations of core and faces could differ. Zuo and Hjelmstad [4] extended Krajcinovic's warping theory to *n*-layer bonded beams and corresponding static governing equations were derived. A closed-form solution was presented and the interfacial shear stress

was calculated which can be used to predict delamination failures. Banerjee *et al*, [5] in his earlier work assumed that the top and the bottom layers of the sandwich beam behave according to the Bernoulli-Euler beam theory whereas the core deforms only in shear. Later, Banerjee and Sobey [6] improved the model by idealizing the top and bottom layers as Rayleigh beams, whereas the central core as a Timoshenko beam. In a recent paper, Banerjee *et al*. [7] advanced the sandwich beam model by assuming each layer as a Timoshenko beam. Atlihan *et al*. [8] developed a differential quadrature method (DQM) model for the vibration analysis of a laminated composite beam, for which Bernoulli-Euler hypothesis is assumed. Lee [9] developed a model for the free vibration analysis of a laminated beam with delamination using layerwise theory and developed a finite element method.

All above theories laid solid foundation for the analysis of multi-layered beams. However, conventional finite element solution approach requires very fine mesh particularly for the damage zone, which significantly increases the computational cost at high frequencies. As it is shown in Figure 1-1, both CLPT and FSDT are more suitable for modal analysis. However, in order to capture the wave propagation characteristics of a multi-layered structure, a higher order model, which includes the warping effects, is needed. Therefore, an accurate dynamic model and an efficient solution approach are equally important to accurately and efficiently capture the wave propagation characteristics in a multi-layered beam.

1.3 Introduction to Spectral Finite Element Method

A solid understanding of the dynamic behavior and characteristics of a structure is of great importance in engineering, and the conventional finite element method (CFEM) has been used extensively in the dynamic analysis of such systems. CFEM is a numerical technique for finding

approximate solutions to partial differential equations (PDE) and their systems and it has been used by many researchers [10-12] to study the wave propagation in structures. In CFEM, a complicated system is divided into smaller elements, and then they are solved in relation to each other. The dynamic behavior of a structure depends on the vibration frequency, and its wavelength, which is very small at high frequency, and in order to obtain accurate wave propagation prediction, large number of elements must be used. Typically, the size of an element needs to be 10-20 times smaller than the wavelength [13]. In addition, conventional finite element models are formulated by using frequency independent (static or fixed) polynomial shape (interpolation) functions, which are inefficient at capturing necessary high frequency modes.

The aforementioned limitations of finite element method can be overcome by refining the mesh; however, this approach usually results in an extremely large system, which is also very computational expensive. As the refinement of mesh is not an effective solution to increase the solution accuracy, as an alternate approach, shape functions that can vary depending on the vibration frequency can be used. Such shape functions are also known as dynamic shape functions in the literature, and since they can capture necessary high frequency modes, extremely accurate solutions can be obtained, and mesh refinement is also no longer necessary.

Spectral Finite Element Method (SFEM) is a technique that can provide high fidelity predictions using comparatively small number of elements. It was initially introduced by Narayanan and Beskos [14], and has been in existence for a long time under the name of the dynamic stiffness matrix by Doyle [13], Leung [15], Gopalakrishnan [16]. The solution procedure of SFEM is similar to CFEM, but the difference is that SFEM is formulated in frequency domain and its interpolation functions are exact solutions of the governing equations, hence providing the ability

to deal with high frequency problems where the wavelengths become very small [16]. Since the mass distribution within the structural element is treated exactly, any regular part of the structure can be modeled with a single element, resulting in significant reduction in the number of elements to define a problem compared to CFEM. This methodology has been successfully demonstrated in one dimensional isotropic structure [17-20].

Exact dynamic shape functions that are derived from exact wave solutions to the governing differential equations are used to formulate dynamic stiffness matrix. To obtain the exact wave solutions in the frequency domain, the time-domain governing differential equations are first transformed into the frequency domain. As a result of this transformation, the exact dynamic stiffness matrix is also frequency dependent and it automatically deals with the continuous mass distribution in a structural element. Thus, the need for subdividing a structural member into smaller elements is eliminated, and only a single element is sufficient to model a regular part of a structure provided that there are no structural or material discontinuities. A new element is introduced only at discontinuities, therefore structural models use substantially less number of elements compared to conventional FEM. Consequently, the size of the problem, in other words, the total number of elements, and subsequently degrees-of-freedom (DOFs), will be significantly reduced, which will result in significantly less amount of computational cost and time.

Dynamic stiffness matrices are stiffness formulated and similar to the conventional finite element method, total dynamic stiffness matrix can be assembled in a completely similar way to that is used in the FEM to yield the following linear equation in terms of nodal displacement and the corresponding force vectors.

$$\hat{F} = D(\omega)\hat{u} \tag{1}$$

Because the dynamic stiffness matrices are derived in frequency domain, the total dynamic stiffness matrix is also a function of frequency. This requires the force vector on the left hand side of Eq. (1) to be defined in frequency domain as well. This is accomplished by conducting FFT for the applied force defined in the time domain. Then the nodal displacement vector can be solved accordingly. Finally, the transient response can be calculated by conducting inverse FFT.

Various spectral element models have been developed for composite beams. Mahapatra et al. [21] developed the spectral finite element method for Euler-Bernoulli beam. Mahapatra and Gopalakrishnan [22] and Ruotolo [23] have developed the spectral finite element method for Timoshenko beam. Palacz et al. [24] presented a spectral finite element medel for analysis of flexural-shear coupled wave propagation in laminated composite beams according to the FSDT. A spectrally formulated wavelet finite element considering thickness deformability was developed by Mitra and Gopalakrishnan [25] to study the axial-flexure-shear coupled wave propagation in composite beams. Peng et al. [26] analyzed wave propagation characteristics of laminated composite beams in intact and delaminated states using the spectral element method based on the CLT. Lee and Jang [27] developed a spectral element model for an axially loaded bending-shear-torsion coupled composite laminated beam which was based on FSDT.

Krawczuk [28] developed a spectral element of a cracked Timoshenko beam, and demonstrated the influence of crack parameters on the wave propagation. Banerjee also used spectral element method to analyze the modal characteristics of a three layer sandwich beam. Efficiency and effectiveness of spectral element method over classical finite element method have been clearly demonstrated in these research efforts.

1.4 Current Research Scope

The main focus of this study is to develop and code a spectral finite element model for an n-layered elastic beam, and investigate its dynamic and wave propagation characteristics. A model based on Zig-Zag theory is developed, and then a spectral element is developed based on this model. The developed spectral element is then verified by literature results and compared with the results obtained from the CFEM. The final demonstration is to develop a damage detection scheme to relate wave propagation characteristics to identify the damage location and assess damage extend on a beam structure.

The thesis is organized as follows. Chapter 0 details the development of a higher order multi-layered model (MLM). Each layer of the beam will be idealized as a Timoshenko beam to include warping effects. The energy expressions of the multi-layered beam will be formulated using theory of elasticity. Then Hamilton's principle will be applied to derive the governing differential equations of motion and associated natural boundary conditions. In Chapter 0 a Spectral Finite Element Model (SFEM) is developed for the multi-layered model. By using harmonic oscillation, the differential equations will be combined into a state space model, and solved in closed analytical form. Then the frequency dependent dynamic stiffness matrix of the system will be derived by relating the amplitudes of the axial and shear forces, and bending moments to those of the axial and transversal displacements and bending rotations. Chapter 0 documents all the model verifications and results obtained from simulations. The dynamic stiffness matrix derived in the previous step will be used in the analysis. In addition, conventional FEM will also be performed with NASTRAN, and Frequency Response Function (FRF) of SFEM and FEM will be compared for the accuracy, as well as to illustrate the efficiency of the developed SFEM. Then wave propagation response for a cantilevered beam

under a high frequency impulse excitation will be analyzed. The main purpose will be the investigation of if the damage and the extent of the damage in the structure can be identified using the developed SFEM. And finally, the effect of excitation frequency on damage detection will be investigated. The developed SFEM will be used with different excitation frequencies on a model, and response characteristics will be compared to determine the effects on the damage detection scheme. Chapter 0 includes concluding remarks on the thesis and the proposed future work.

Modal Analysis

Wave Analysis

Classical Laminated Plate Theory*
(CLPT)

First-Order Shear Deformation Theory*
(FSDT)

Multi-layered Model
(Zig-Zag Kinematics**)
(MLM)

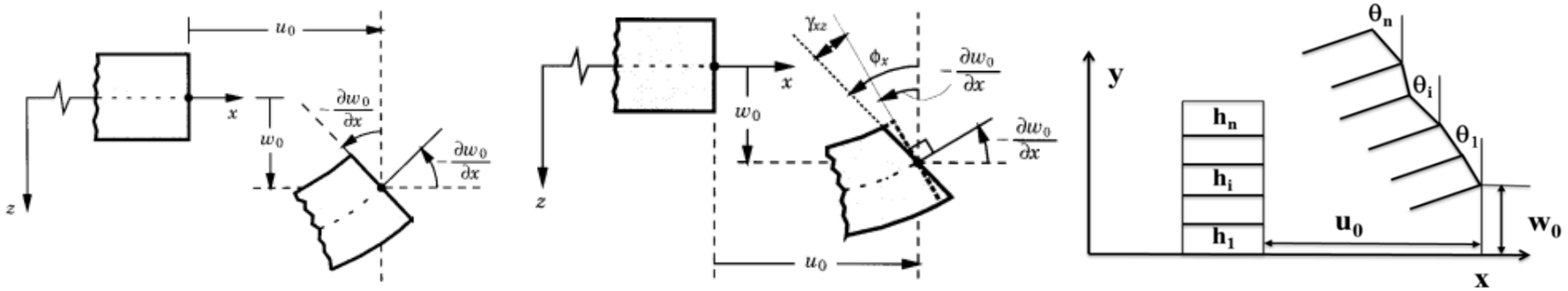

Figure 1. Comparison of Different Beam Theories

CHAPTER 2

MODEL DEVELOPMENT

In this chapter, a mathematical model of a multi-layered beam will be developed. Governing differential equations will be derived, and consequently solved using state space method in order to formulate the SFEM.

This chapter is divided into four sections. In the first section kinematics of the model will be examined. Axial displacement for each layer will be expressed, and followed by normal and shear strain definitions for each layer. In the second section, the model will be developed by using the total potential energy, kinetic energy and external work done on the system defined. In the third section, Hamilton's principle is implemented to obtain the governing differential equations and associated boundary conditions. Finally, in section four, Timoshenko Beam equations are shown using the governing differential equations derived.

2.1 Kinematics

Figure 2 shows a composite beam made of n layers of elastic materials. Here, u_0 is the axial displacement at the bottom of the first lamina, h_i and θ_i are the height and the rotation of the i^{th} lamina, respectively. Typically the axial displacement is selected at the middle of the layer. However, this leads to a lengthy expression of the governing equations as it is demonstrated in Ref [27]. By choosing the displacement at the bottom of the first layer, kinematic expression of each layer becomes simpler and it is possible to achieve a compact form of governing equations.

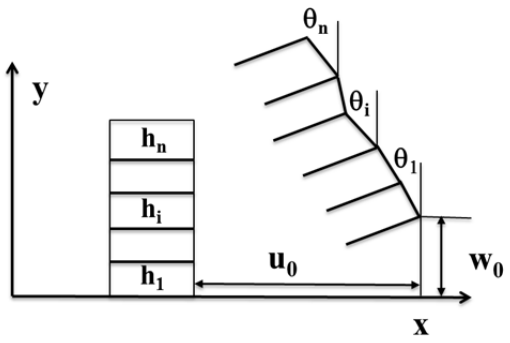

Figure 2. Kinematics

Key assumptions in the analysis are listed below:

- The axial displacement at the bottom of the first layer is introduced and displacement compatibility conditions are applied accordingly. (i.e., no slip between layers).
- Transversal deformation is neglected, i.e., constant transverse displacement across the height of the whole cross-sectional of the beam is assumed.
- The cross-section of each layer remains planar after deformation, but the rotations of the individual laminas are allowed, i.e., the warping effects is included.
- Each layer is assumed to have an elastic material with linear material characteristics.

Based on these assumptions, the axial displacement in i^{th} lamina can be expressed as

$$u_i(x,y,t) = u_0(x,t) - \sum_{j=1}^{i-1} h_j \theta_j(x,t) - \left(y - \sum_{j=1}^{i-1} h_j \right) \theta_i(x,t) \qquad (2)$$

The last term in Eq. (2) can be replaced by a local coordinate variable $\bar{y}$ for the i^{th} lamina. It is defined by

$$\bar{y} = y - \sum_{j=1}^{i-1} h_j \tag{3}$$

Then the axial displacement takes the following form

$$u_i(x,y,t) = u_0(x,t) - \sum_{j=1}^{i-1} h_j \theta_j(x,t) - \bar{y}\theta_i(x,t) \tag{4}$$

and the normal strain for the i^{th} lamina is given by

$$\varepsilon_{xx}^{i} = \frac{\partial u_0}{\partial x} - \sum_{j=1}^{i-1} h_j \frac{\partial \theta_j}{\partial x} - \bar{y}\frac{\partial \theta_i}{\partial x} \tag{5}$$

Whereas the shear strain for the i^{th} lamina is given by

$$\varepsilon_{xy}^{i} = \frac{\partial u_i}{\partial y} + \frac{\partial w_i}{\partial x} = \frac{\partial w_0}{\partial x} - \theta_i \tag{6}$$

Here, w_0 is the transverse displacement, which is assumed constant over the height of the entire beam.

2.2 Model

The total strain energy U_i for the i^{th} lamina is

$$U_i = \frac{1}{2}\int_V \left[E_i \left(\varepsilon_{xx}^{i}\right)^2 + G_i \left(\varepsilon_{xy}^{i}\right)^2 \right] dV \tag{7}$$

which can also be expressed as

$$U_i = \frac{1}{2}\int_0^L \int_0^{h_i} b_i \left[E_i \left(\varepsilon_{xx}^{i}\right)^2 + G_i \left(\varepsilon_{xy}^{i}\right)^2 \right] d\bar{y}\, dx \tag{8}$$

where b_i is the width of the i^{th} lamina. Substituting Eq. (5) and (6) into Eq.(8), and by carrying out the integration with respect to $\bar{y}$, we obtain

$$U_i = \frac{1}{2}\int_0^L \left[\begin{array}{l} E_i b_i h_i \left[\left(\frac{\partial u_0}{\partial x} \right)^2 - 2\left(\frac{\partial u_0}{\partial x} \right) \sum_{j=1}^{i-1} \left(h_j \frac{\partial \theta_j}{\partial x} \right) + \left(\sum_{j=1}^{i-1} h_j \frac{\partial \theta_j}{\partial x} \right)^2 \right] - E_i b_i h_i^2 \frac{\partial u_0}{\partial x} \frac{\partial \theta_i}{\partial x} \\ + E_i b_i h_i^2 \left(\sum_{j=1}^{i-1} h_j \frac{\partial \theta_j}{\partial x} \right) \frac{\partial \theta_i}{\partial x} + E_i b_i \frac{h_i^3}{3} \left(\frac{\partial \theta_i}{\partial x} \right)^2 + G_i b_i h_i \left[\left(\frac{\partial w_0}{\partial x} \right)^2 - 2\frac{\partial w_0}{\partial x}\theta_i + (\theta_i)^2 \right] \end{array} \right] dx \qquad (9)$$

which can be simplified by using

$$(EA)_i = E_i b_i h_i \qquad (10)$$

$$(GA)_i = G_i b_i h_i \qquad (11)$$

From parallel axis theorem, moment of inertia, I_i for i^{th} lamina

$$I_i = I_i^c + b_i h_i \left(\frac{h_i}{2} \right)^2 = I_i^c + \frac{b_i h_i^3}{4} \qquad (12)$$

Where

$$I_i^c = \frac{1}{12} b_i h_i^3 \qquad (13)$$

Substituting Eq. (13) into Eq. (12), we obtain the moment of inertia for i^{th} lamina in the following form

$$I_i = \frac{1}{3} b_i h_i^3 \qquad (14)$$

By using Eq. (14), bending stiffness for i^{th} lamina, $(EI)_i$ can be expressed in the following way

$$(EI)_i = E_i b_i \frac{h_i^3}{3} \tag{15}$$

By using Eq. (10), Eq. (11), and Eq. (15), we obtain the final equation for total strain energy

$$U_i = \frac{1}{2}\int_0^L \left[\begin{array}{c} (EA)_i \left[\left(\frac{\partial u_0}{\partial x} \right)^2 - 2\left(\frac{\partial u_0}{\partial x} \right) \sum_{j=1}^{i-1} \left(h_j \frac{\partial \theta_j}{\partial x} \right) + \left(\sum_{j=1}^{i-1} h_j \frac{\partial \theta_j}{\partial x} \right)^2 \right] \\ + (EA)_i h_i \left[\left(\sum_{j=1}^{i-1} h_j \frac{\partial \theta_j}{\partial x} \right) \frac{\partial \theta_i}{\partial x} - \frac{\partial u_0}{\partial x} \frac{\partial \theta_i}{\partial x} \right] \\ + (EI)_i \left(\frac{\partial \theta_i}{\partial x} \right)^2 + (GA)_i \left[\left(\frac{\partial w_0}{\partial x} \right)^2 - 2 \frac{\partial w_0}{\partial x} \theta_i + (\theta_i)^2 \right] \end{array} \right] dx \tag{16}$$

The kinetic energy of the i^{th} lamina can be expressed as

$$T_i = \frac{1}{2}\int_0^L dx \int_0^{h_i} \left[\rho_i \left(\dot{u}_i^c \right)^2 + \rho_i I_i^c \left(\dot{\theta}_i \right)^2 + \rho_i \left(\dot{w}_0 \right)^2 \right] b_i d\bar{y} \tag{17}$$

where ρ_i is the density of i^{th} layer's material, and the first, second and third terms in (17) are axial, rotational and transverse kinetic energy terms for each lamina. The velocity of the center of i^{th} layer, $\dot{u}_i^c$ in Eq. (17) can be obtained by substituting

$$\bar{y} = \frac{h_i}{2} \tag{18}$$

into Eq. (4), which yields

$$\dot{u}_i^c = \dot{u}_0 - \sum_{j=1}^{i-1} h_j \dot{\theta}_j - \frac{h_i}{2} \dot{\theta}_i \tag{19}$$

$\left(\dot{u}_i^c \right)^2$ term in Eq. (17) can be expanded using Eq. (19) in the following way,

$$\left(\dot{u}_i^c\right)^2 = \left(\dot{u}_0\right)^2 - 2\dot{u}_0\left(\sum_{j=1}^{i-1} h_j\dot{\theta}_j + \frac{h_i}{2}\dot{\theta}_i\right) + \left(\sum_{j=1}^{i-1} h_j\dot{\theta}_j\right)h_i\dot{\theta}_i + \left(\sum_{j=1}^{i-1} h_j\dot{\theta}_j\right)^2 + \frac{h_i^2}{4}\dot{\theta}_i^2 \tag{20}$$

and substituting into Eq. (17), integrating with respect to $\bar{y}$, and rearranging the terms,

$$T_i = \frac{1}{2}\int_0^L \left[m_i\left[\dot{u}_0{}^2 - 2\dot{u}_0\left(\sum_{j=1}^{i-1} h_j\dot{\theta}_j + \frac{h_i}{2}\dot{\theta}_i\right) + \left(\sum_{j=1}^{i-1} h_j\dot{\theta}_j\right)h_i\dot{\theta}_i + \left(\sum_{j=1}^{i-1} h_j\dot{\theta}_j\right)^2 + \frac{h_i^2}{4}\dot{\theta}_i^2 \right] + m_i I_i^c\dot{\theta}_i^2 + m_i\dot{w}_0{}^2 \right] dx \tag{21}$$

Where m_i is the mass per unit length, and it is defined as

$$m_i = \rho_i b_i h_i \tag{22}$$

Finally, the virtual work is defined as

$$\delta W = \int_0^L q\,\delta W_0 dx \tag{23}$$

Final form of total potential energy is given by

$$U = \sum_{i=1}^{n} U_i = \frac{1}{2}\int_0^L \sum_{i=1}^{n} \left[\begin{array}{l} \left(EA\right)_i\left[\dfrac{\partial u_0}{\partial x}^2 - 2\dfrac{\partial u_0}{\partial x}\sum_{j=1}^{i-1} h_j\dfrac{\partial\theta_j}{\partial x} + \left(\sum_{j=1}^{i-1} h_j\dfrac{\partial\theta_j}{\partial x}\right)^2 \right] \\ + \left(EA\right)_i h_i\left[\left(\sum_{j=1}^{i-1} h_j\dfrac{\partial\theta_j}{\partial x}\right)\dfrac{\partial\theta_i}{\partial x} - \dfrac{\partial u_0}{\partial x}\dfrac{\partial\theta_i}{\partial x} \right] + \left(EI\right)_i\left(\dfrac{\partial\theta_i}{\partial x}\right)^2 \\ + \left(GA\right)_i\left[\dfrac{\partial w_0}{\partial x}^2 - 2\dfrac{\partial w_0}{\partial x}\theta_i + \theta_i^2 \right] \end{array} \right] dx \tag{24}$$

whereas final form of the total kinetic energy is given by

$$T = \sum_{i=1}^{n} T_i = \frac{1}{2}\int_0^L \sum_{i=1}^{n} \left[\begin{array}{c} m_i\left(\dot{u}_0{}^2 - 2\dot{u}_0 \sum_{j=1}^{i-1} h_j\dot{\theta}_j + \left(\sum_{j=1}^{i-1} h_j\dot{\theta}_j \right)^2 \right) - m_i h_i \dot{u}_0 \dot{\theta}_i \\ + m_i h_i \left(\sum_{j=1}^{i-1} h_j\dot{\theta}_j \right)\dot{\theta}_i + J_i\dot{\theta}_i{}^2 + m_i\dot{w}_0{}^2 \end{array} \right] dx \tag{25}$$

where

$$J_i = \left(I_i^c + \frac{h_i^2}{4} \right) m_i \tag{26}$$

Hamilton's Principle can now be applied to obtain governing equations.

$$\int_{t_1}^{t_2} \delta(T - U + W)dt = 0 \tag{27}$$

2.3 Governing Equations

2.3.1 Derivation

Each term in Eq. (27) is calculated separately, as they are shown in the following sections. Starting with potential energy term,

$$\int_{t_1}^{t_2}\delta U dt=\int_{t_1}^{t_2}dt\int_0^L\sum_{i=1}^{n}\left[\begin{array}{l}(EA)_i\left[\begin{array}{l}\dfrac{\partial u_0}{\partial x}\delta\dfrac{\partial u_0}{\partial x}-\dfrac{\partial u_0}{\partial x}\displaystyle\sum_{j=1}^{i-1}h_j\delta\dfrac{\partial\theta_j}{\partial x}-\left(\displaystyle\sum_{j=1}^{i-1}h_j\dfrac{\partial\theta_j}{\partial x}\right)\delta\dfrac{\partial u_0}{\partial x}\\ \qquad\qquad+\left(\displaystyle\sum_{j=1}^{i-1}h_j\dfrac{\partial\theta_j}{\partial x}\right)\displaystyle\sum_{j=1}^{i-1}h_j\delta\dfrac{\partial\theta_j}{\partial x}\end{array}\right]\\ +(EA)_i\dfrac{h_i}{2}\left[\begin{array}{l}\left(\displaystyle\sum_{j=1}^{i-1}h_j\dfrac{\partial\theta_j}{\partial x}\right)\delta\dfrac{\partial\theta_i}{\partial x}\\ +\left(\displaystyle\sum_{j=1}^{i-1}h_j\left(\delta\dfrac{\partial\theta_j}{\partial x}\right)\right)\dfrac{\partial\theta_i}{\partial x}-\dfrac{\partial u_0}{\partial x}\delta\dfrac{\partial\theta_i}{\partial x}-\delta\dfrac{\partial u_0}{\partial x}\dfrac{\partial\theta_i}{\partial x}\end{array}\right]\\ +(EI)_i\dfrac{\partial\theta_i}{\partial x}\delta\dfrac{\partial\theta_i}{\partial x}\\ +(GA)_i\left[\dfrac{\partial w_0}{\partial x}\delta\dfrac{\partial w_0}{\partial x}-\dfrac{\partial w_0}{\partial x}\delta\theta_i-\theta_i\delta\dfrac{\partial w_0}{\partial x}+\theta_i\delta\theta_i\right]\end{array}\right]dx \tag{28}$$

The derivative in the variational needs to be eliminated, which can be accomplished by integration by parts, as it is shown in Eq. (29).

$$
\int_{t_1}^{t_2}\delta U dt = \left[\begin{array}{l}
\int_{t_1}^{t_2}\left(\sum_{i=1}^{n}(EA)_i\frac{\partial u_0}{\partial x}\delta u_0\Big|_0^L\right)dt-\int_{t_1}^{t_2}dt\int_0^L\left(\sum_{i=1}^{n}(EA)_i\frac{\partial^2 u_0}{\partial x^2}\delta u_0\right)dx \\
-\int_{t_1}^{t_2}\left(\sum_{i=1}^{n}(EA)_i\frac{\partial u_0}{\partial x}\sum_{j=1}^{i-1}h_j\delta\theta_j\Big|_0^L\right)dt+\int_{t_1}^{t_2}dt\int_0^L\left(\sum_{i=1}^{n}(EA)_i\frac{\partial^2 u_0}{\partial x^2}\sum_{j=1}^{i-1}h_j\delta\theta_j\right)dx \\
-\int_{t_1}^{t_2}\left(\sum_{i=1}^{n}(EA)_i\sum_{j=1}^{i-1}h_j\frac{\partial\theta_j}{\partial x}\delta u_0\Big|_0^L\right)dt+\int_{t_1}^{t_2}dt\int_0^L\left(\sum_{i=1}^{n}(EA)_i\sum_{j=1}^{i-1}h_j\frac{\partial^2\theta_j}{\partial x^2}\delta u_0\right)dx \\
+\int_{t_1}^{t_2}\left(\sum_{i=1}^{n}(EA)_i\sum_{j=1}^{i-1}h_j\frac{\partial\theta_j}{\partial x}\sum_{j=1}^{i-1}h_j\delta\theta_j\Big|_0^L\right)dt-\int_{t_1}^{t_2}dt\int_0^L\left(\sum_{i=1}^{n}(EA)_i\sum_{j=1}^{i-1}h_j\frac{\partial^2\theta_j}{\partial x^2}\sum_{j=1}^{i-1}h_j\delta\theta_j\right)dx \\
+\int_{t_1}^{t_2}\left(\sum_{i=1}^{n}(EA)_i\frac{h_i}{2}\sum_{j=1}^{i-1}h_j\frac{\partial\theta_j}{\partial x}\delta\theta_i\Big|_0^L\right)dt-\int_{t_1}^{t_2}dt\int_0^L\left(\sum_{i=1}^{n}(EA)_i\frac{h_i}{2}\sum_{j=1}^{i-1}h_j\frac{\partial^2\theta_j}{\partial x^2}\delta\theta_i\right)dx \\
+\int_{t_1}^{t_2}\left(\sum_{i=1}^{n}(EA)_i\frac{h_i}{2}\frac{\partial\theta_i}{\partial x}\sum_{j=1}^{i-1}h_j\delta\theta_j\Big|_0^L\right)dt-\int_{t_1}^{t_2}dt\int_0^L\left(\sum_{i=1}^{n}(EA)_i\frac{h_i}{2}\frac{\partial^2\theta_i}{\partial x^2}\sum_{j=1}^{i-1}h_j\delta\theta_j\right)dx \\
-\int_{t_1}^{t_2}\left(\sum_{i=1}^{n}(EA)_i\frac{h_i}{2}\frac{\partial u_0}{\partial x}\delta\theta_i\Big|_0^L\right)dt+\int_{t_1}^{t_2}dt\int_0^L\left(\sum_{i=1}^{n}(EA)_i\frac{h_i}{2}\frac{\partial^2 u_0}{\partial x^2}\delta\theta_i\right)dx \\
-\int_{t_1}^{t_2}\left(\sum_{i=1}^{n}(EA)_i\frac{h_i}{2}\frac{\partial\theta_i}{\partial x}\delta u_0\Big|_0^L\right)dt+\int_{t_1}^{t_2}dt\int_0^L\left(\sum_{i=1}^{n}(EA)_i\frac{h_i}{2}\frac{\partial^2\theta_i}{\partial x^2}\delta u_0\right)dx \\
+\int_{t_1}^{t_2}\left(\sum_{i=1}^{n}(EI)_i\frac{\partial\theta_i}{\partial x}\delta\theta_i\Big|_0^L\right)dt-\int_{t_1}^{t_2}dt\int_0^L\left(\sum_{i=1}^{n}(EI)_i\frac{\partial^2\theta_i}{\partial x^2}\delta\theta_i\right)dx \\
+\int_{t_1}^{t_2}\left(\sum_{i=1}^{n}(GA)_i\frac{\partial w_0}{\partial x}\delta w_0\Big|_0^L\right)dt-\int_{t_1}^{t_2}dt\int_0^L\left(\sum_{i=1}^{n}(GA)_i\frac{\partial^2 w_0}{\partial x^2}\delta w_0\right)dx \\
-\int_{t_1}^{t_2}dt\int_0^L\left(\sum_{i=1}^{n}(GA)_i\frac{\partial w_0}{\partial x}\delta\theta_i\right)dx \\
-\int_{t_1}^{t_2}\left(\sum_{i=1}^{n}(GA)_i\theta_i\delta w_0\Big|_0^L\right)dt+\int_{t_1}^{t_2}dt\int_0^L\left(\sum_{i=1}^{n}(GA)_i\frac{\partial\theta_i}{\partial x}\delta w_0\right)dx \\
+\int_{t_1}^{t_2}dt\int_0^L\left(\sum_{i=1}^{n}(GA)_i\theta_i\delta\theta_i\right)dx
\end{array}\right] \tag{29}
$$

$$\int_{t_1}^{t_2}\delta T dt=\int_{t_1}^{t_2}dt\int_0^L\sum_{i=1}^{n}\left[\begin{array}{c} m_i\dot{u}_0\delta\dot{u}_0-m_i\dot{u}_0\sum_{j=1}^{i-1}h_j\delta\dot{\theta}_j-m_i\left(\sum_{j=1}^{i-1}h_j\dot{\theta}_j\right)\delta\dot{u}_0+m_i\sum_{j=1}^{i-1}h_j\dot{\theta}_j\sum_{j=1}^{i-1}h_j\delta\dot{\theta}_j \\ -m_i\frac{h_i}{2}\dot{\theta}_i\delta\dot{u}_0-m_i\frac{h_i}{2}\dot{u}_0\delta\dot{\theta}_i+m_i\frac{h_i}{2}\left(\sum_{j=1}^{i-1}h_j\dot{\theta}_j\right)\delta\dot{\theta}_i+m_i\frac{h_i}{2}\dot{\theta}_i\sum_{j=1}^{i-1}h_j\delta\dot{\theta}_j \\ +J_i\dot{\theta}_i\delta\dot{\theta}_i+m_i\dot{w}_0\delta\dot{w}_0 \end{array}\right]dx \tag{30}$$

Again, the derivative in the variational needs to be eliminated, which can be accomplished by integration by parts.

$$\int_{t_1}^{t_2}\delta T dt=\left[\begin{array}{l} \int_0^L\left(\sum_{i=1}^{n}m_i\dot{u}_0\delta u_0\Big|_{t_1}^{t_2}\right)dx-\int_{t_1}^{t_2}dt\int_0^L\left(\sum_{i=1}^{n}m_i\ddot{u}_0\delta u_0\right)dx \\ -\int_0^L\left(\sum_{i=1}^{n}m_i\dot{u}_0\sum_{j=1}^{i-1}h_j\delta\theta_j\Big|_{t_1}^{t_2}\right)dx+\int_{t_1}^{t_2}dt\int_0^L\left(\sum_{i=1}^{n}m_i\ddot{u}_0\sum_{j=1}^{i-1}h_j\delta\theta_j\right)dx \\ -\int_0^L\left(\sum_{i=1}^{n}m_i\left(\sum_{j=1}^{i-1}h_j\dot{\theta}_j\right)\delta u_0\Big|_{t_1}^{t_2}\right)dx+\int_{t_1}^{t_2}dt\int_0^L\left(\sum_{i=1}^{n}m_i\left(\sum_{j=1}^{i-1}h_j\ddot{\theta}_j\right)\delta u_0\right)dx \\ +\int_0^L\left(\sum_{i=1}^{n}m_i\left(\sum_{j=1}^{i-1}h_j\dot{\theta}_j\right)\left(\sum_{j=1}^{i-1}h_j\delta\theta_j\right)\Big|_{t_1}^{t_2}\right)dx-\int_{t_1}^{t_2}dt\int_0^L\left(\sum_{i=1}^{n}m_i\left(\sum_{j=1}^{i-1}h_j\ddot{\theta}_j\right)\left(\sum_{j=1}^{i-1}h_j\delta\theta_j\right)\right)dx \\ -\int_0^L\left(\sum_{i=1}^{n}m_i\frac{h_i}{2}\dot{\theta}_i\delta u_0\Big|_{t_1}^{t_2}\right)dx+\int_{t_1}^{t_2}dt\int_0^L\left(\sum_{i=1}^{n}m_i\frac{h_i}{2}\ddot{\theta}_i\delta u_0\right)dx \\ -\int_0^L\left(\sum_{i=1}^{n}m_i\frac{h_i}{2}\dot{u}_0\delta\theta_i\Big|_{t_1}^{t_2}\right)dx+\int_{t_1}^{t_2}dt\int_0^L\left(\sum_{i=1}^{n}m_i\frac{h_i}{2}\ddot{u}_0\delta\theta_i\right)dx \\ +\int_0^L\left(\sum_{i=1}^{n}m_i\frac{h_i}{2}\left(\sum_{j=1}^{i-1}h_j\dot{\theta}_j\right)\delta\theta_i\Big|_{t_1}^{t_2}\right)dx-\int_{t_1}^{t_2}dt\int_0^L\left(\sum_{i=1}^{n}m_i\frac{h_i}{2}\left(\sum_{j=1}^{i-1}h_j\ddot{\theta}_j\right)\delta\theta_i\right)dx \\ +\int_0^L\left(\sum_{i=1}^{n}m_i\frac{h_i}{2}\dot{\theta}_i\sum_{j=1}^{i-1}h_j\delta\theta_j\Big|_{t_1}^{t_2}\right)dx-\int_{t_1}^{t_2}dt\int_0^L\left(\sum_{i=1}^{n}m_i\frac{h_i}{2}\ddot{\theta}_i\sum_{j=1}^{i-1}h_j\delta\theta_j\right)dx \\ +\int_0^L\left(\sum_{i=1}^{n}J_i\dot{\theta}_i\delta\theta_i\Big|_{t_1}^{t_2}\right)dx-\int_{t_1}^{t_2}dt\int_0^L\left(\sum_{i=1}^{n}J_i\ddot{\theta}_i\delta\theta_i\right)dx \\ +\int_0^L\left(\sum_{i=1}^{n}m_i\dot{w}_0\delta w_0\Big|_{t_1}^{t_2}\right)dx-\int_{t_1}^{t_2}dt\int_0^L\left(\sum_{i=1}^{n}m_i\ddot{w}_0\delta w_0\right)dx \end{array}\right] \tag{31}$$

Now that each $\int_{t_1}^{t_2}\delta T dt$ and $\int_{t_1}^{t_2}\delta U dt$ are calculated in Eq. (27), collecting δu_0 in $T-U$ will yield the first governing equation:

$$\int_{t_1}^{t_2}dt\int_0^L\sum_{i=1}^{n}\left[\begin{array}{r}-m_i\ddot{u}_0+m_i\left(\sum_{j=1}^{i-1}h_j\ddot{\theta}_j\right)+m_i\frac{h_i}{2}\ddot{\theta}_i+(EA)_i\frac{\partial^2u_0}{\partial x^2}-(EA)_i\left(\sum_{j=1}^{i-1}h_j\frac{\partial^2\theta_j}{\partial x^2}\right)\\ -(EA)_i\frac{h_i}{2}\frac{\partial^2\theta_i}{\partial x^2}\end{array}\right]\delta u_0dx=0 \tag{32}$$

Collect δw_0 to obtain second governing equation:

$$\int_{t_1}^{t_2}dt\int_0^L\sum_{i=1}^{n}\left[-m_i\ddot{w}_0+(GA)_i\frac{\partial^2w_0}{\partial x^2}-(GA)_i\frac{\partial\theta_i}{\partial x}+q\right]\delta w_0dx=0 \tag{33}$$

And finally collect θ_i and $\sum_{j=1}^{i-1}h_j\theta_j$ in $T-U$ to obtain the third governing equation:

$$\int_{t_1}^{t_2}dt\int_0^L\sum_{i=1}^{n}\left[\begin{array}{r}m_i\ddot{u}_0\sum_{j=1}^{i-1}h_j\delta\theta_j-m_i\sum_{j=1}^{i-1}h_j\ddot{\theta}_j\sum_{j=1}^{i-1}h_j\delta\theta_j+m_i\frac{h_i}{2}\ddot{u}_0\delta\theta_i-m_i\frac{h_i}{2}\left(\sum_{j=1}^{i-1}h_j\ddot{\theta}_j\right)\delta\theta_i\\ -m_i\frac{h_i}{2}\ddot{\theta}_i\sum_{j=1}^{i-1}h_j\delta\theta_j-J_i\ddot{\theta}_i\delta\theta_i-(EA)_i\frac{\partial^2u_0}{\partial x^2}\left(\sum_{j=1}^{i-1}h_j\delta\theta_j\right)\\ +(EA)_i\sum_{j=1}^{i-1}h_j\frac{\partial^2\theta_j}{\partial x^2}\sum_{j=1}^{i-1}h_j\delta\theta_j+(EA)_i\frac{h_i}{2}\left(\sum_{j=1}^{i-1}h_j\frac{\partial^2\theta_j}{\partial x^2}\right)\delta\theta_i+(EA)_i\frac{h_i}{2}\frac{\partial^2\theta_i}{\partial x^2}\sum_{j=1}^{i-1}h_j\delta\theta_j\\ -(EA)_i\frac{h_i}{2}\frac{\partial^2u_0}{\partial x^2}\delta\theta_i+(EI)_i\frac{\partial^2\theta_i}{\partial x^2}\delta\theta_i+(GA)_i\frac{\partial w_0}{\partial x}\delta\theta_i-(GA)_i\theta_i\delta\theta_i\end{array}\right]dx=0 \tag{34}$$

$$\int_{t_1}^{t_2}dt\int_0^L\sum_{i=1}^{n}\left[\begin{array}{r}\left[m_i\ddot{u}_0-m_i\sum_{j=1}^{i-1}h_j\ddot{\theta}_j-m_i\frac{h_i}{2}\ddot{\theta}_i-(EA)_i\frac{\partial^2u_0}{\partial x^2}\right]\sum_{j=1}^{i-1}h_j\delta\theta_j\\ +(EA)_i\sum_{j=1}^{i-1}h_j\frac{\partial^2\theta_j}{\partial x^2}+(EA)_i\frac{h_i}{2}\frac{\partial^2\theta_i}{\partial x^2}\\ +\left[m_i\frac{h_i}{2}\ddot{u}_0-m_i\frac{h_i}{2}\sum_{j=1}^{i-1}h_j\ddot{\theta}_j-J_i\ddot{\theta}_i+(EA)_i\frac{h_i}{2}\sum_{j=1}^{i-1}h_j\frac{\partial^2\theta_j}{\partial x^2}-(EA)_i\frac{h_i}{2}\frac{\partial^2u_0}{\partial x^2}\right.\\ \left.+(EI)_i\frac{\partial^2\theta_i}{\partial x^2}+(GA)_i\left[\frac{\partial w_0}{\partial x}-\theta_i\right]\right]\delta\theta_i\end{array}\right]dx=0 \tag{35}$$

2.3.2 Summary of Governing Equations

Equation 1

$$\sum_{i=1}^{n}\left[-m_i\ddot{u}_0+m_i\left(\sum_{j=1}^{i-1}h_j\ddot{\theta}_j\right)+m_i\frac{h_i}{2}\ddot{\theta}_i+(EA)_i\frac{\partial^2 u_0}{\partial x^2}-(EA)_i\left(\sum_{j=1}^{i-1}h_j\frac{\partial^2\theta_j}{\partial x^2}\right)-(EA)_i\frac{h_i}{2}\frac{\partial^2\theta_i}{\partial x^2}\right]=0 \tag{36}$$

Equation 2

$$\sum_{i=1}^{n}\left[(GA)_i\frac{\partial^2 w_0}{\partial x^2}-(GA)_i\frac{\partial\theta_i}{\partial x}-m_i\ddot{w}_0+q\right]=0 \tag{37}$$

Equation 3

$$\sum_{i=1}^{n}\left[(EI^c)_i\frac{\partial^2\theta_i}{\partial x^2}-h_i\left(\frac{1}{2}\frac{\partial N_i^c}{\partial x}+\sum_{j=i+1}^{n}\frac{\partial N_j^c}{\partial x}\right)+(GA)_i\left(\frac{\partial w_0}{\partial x}-\theta_i\right)-\rho_i I_i^c\ddot{\theta}_i+h_i\left(\frac{1}{2}m_i\ddot{u}_i^c+\sum_{j=i+1}^{n}m_j\ddot{u}_j^c\right)\right]=0 \tag{38}$$

With the following boundary conditions

$$N_i=\sum_{i=1}^{n}\left[(EA)_i\varepsilon_{xx}^i\right]=0 \quad or \quad u_0=0 \tag{39}$$

$$V_i=\sum_{i=1}^{n}\left[(GA)_i\varepsilon_{xy}^i\right]=0 \quad or \quad w_0=0 \tag{40}$$

$$M_i=(EI^c)_i\frac{d\theta_i}{dx}-h_i\left(\frac{1}{2}N_i+\sum_{j=i+1}^{n}N_j\right)=0 \quad or \quad \theta_i=0 \tag{41}$$

2.3.3 Example: Governing Equations for a Single Layer Timoshenko Beam

Using governing equation 1;

$$\sum_{i=1}^{n}\left[-m_i\ddot{u}_0+m_i\left(\sum_{j=1}^{i-1}h_j\ddot{\theta}_j\right)+m_i\frac{h_i}{2}\ddot{\theta}_i+(EA)_i\frac{\partial^2 u_0}{\partial x^2}-(EA)_i\left(\sum_{j=1}^{i-1}h_j\frac{\partial^2\theta_j}{\partial x^2}\right)-(EA)_i\frac{h_i}{2}\frac{\partial^2\theta_i}{\partial x^2}\right]=0 \tag{42}$$

We can set $n=1$,

$$-m_1\ddot{u}_0+\frac{1}{2}m_1h_1\ddot{\theta}_i+(EA)_1\frac{\partial^2 u_0}{\partial x^2}-\frac{1}{2}(EA)_1h_1\frac{\partial^2\theta_1}{\partial x^2}=0 \tag{43}$$

Using Equation 2;

$$\sum_{i=1}^{n}\left[(GA)_i\frac{\partial^2 w_0}{\partial x^2}-(GA)_i\frac{\partial\theta_i}{\partial x}-m_i\ddot{w}_0+q\right]=0 \tag{44}$$

We obtain

$$(GA)_1\frac{\partial^2 w_0}{\partial x^2}-(GA)_1\frac{\partial\theta_1}{\partial x}-m_1\ddot{w}_0=0 \tag{45}$$

In Eq. (35), the first part of the vanishes since $n=1$, and the second part of the equation is

$$m_1\frac{h_1}{2}\ddot{u}_0-J_1\ddot{\theta}_1+-(EA)_1\frac{h_1}{2}\frac{\partial^2 u_0}{\partial x^2}+(EI)_1\frac{\partial^2\theta_1}{\partial x^2}+(GA)_1\left[\frac{\partial w_0}{\partial x}-\theta_1\right]=0 \tag{46}$$

Solving (43) for $\ddot{u}_0$ and substituting in (46), we obtain Eq. (47). With Eq. (45) we obtain the two known Timoshenko beam equations:

$$(EI^c)_1\frac{\partial^2\theta_1}{\partial x^2}-J_1^c\ddot{\theta}_1+(GA)_1\left(\frac{\partial w_0}{\partial x}-\theta_1\right)=0 \tag{47}$$

$$(GA)_1\frac{\partial^2 w_0}{\partial x^2}-(GA)_1\frac{\partial\theta_1}{\partial x}-m_1\ddot{w}_0=0 \tag{48}$$

CHAPTER 3

SPECTRAL FINITE ELEMENT FORMULATION

SFEM uses exact dynamic shape functions that are derived from exact wave solutions to the governing differential equations to formulate dynamic stiffness matrix. This allows SFEM to require the least number of elements for the definition of the problem. On the other hand, typical conventional finite element models are formulated by using independent polynomial shape functions, which are inefficient at capturing structure's dynamic behavior at high frequencies. A typical conventional finite element length must be 10-20 times smaller than the wavelength of the highest frequency wave mode to achieve comparable accuracy. This requirement results in increased number of elements, leading to a more computationally expensive system.

In this chapter, Spectral Finite Element is developed for the governing differential equations obtained in the previous chapter. The formulation is carried out in following steps.

3.1 Example: SFEM for a Cantilevered Timoshenko Beam

A spectral finite element model for an isotropic Timoshenko beam is discussed below to illustrate the spectral finite element concept. The governing equation of a Timoshenko beam is given by

$$\rho A \frac{\partial^2 w}{\partial t^2} + GA\kappa\left(\frac{\partial \theta}{\partial x} - \frac{\partial^2 w}{\partial x^2}\right) = 0 \tag{49}$$

$$\rho I \frac{\partial^2 \theta}{\partial t^2} - EI \frac{\partial^2 \theta}{\partial x^2} + GA\kappa\left(\theta - \frac{\partial w}{\partial x}\right) = 0 \tag{50}$$

Where $w(x,t)$ and $\theta(x,t)$ are transverse and angular displacements, respectively. Assume harmonic oscillation, and the solutions are given by

$$w(x,t) = W(x)e^{j\omega t} \tag{51}$$

$$\theta(x,t) = \Theta(x)e^{j\omega t} \tag{52}$$

Substituting Eq. (51)-(52) into Eq. (49)-(50), we obtain

$$GA\kappa\frac{d^2W}{dx^2} - GA\kappa\frac{d\Theta}{dx} + \rho A\omega^2 W = 0 \tag{53}$$

$$EI\frac{d^2\Theta}{dx^2} + GA\kappa\left(\frac{dW}{dx} - \Theta\right) + \rho I\omega^2\Theta = 0 \tag{54}$$

Assume the general solutions to Eq. (53)-(54) are

$$W(x) = \alpha e^{kx} \tag{55}$$

$$\Theta(x) = \beta e^{kx} \tag{56}$$

And substituting Eq. (55)-(56) into (53)-(54), we obtain the following polynomial, which can be used to determine the wave number k

$$(EIGA\kappa)k^4 + (GA\kappa\rho I\omega^2 + EI\rho A\omega^2)k^2 + \rho A\omega^2(\rho I\omega^2 - GA\kappa) = 0 \tag{57}$$

The four roots of the Eq. (57) are

$$k_1 = \sqrt{\frac{-(GA\kappa I + EIA)\rho\omega^2 + \sqrt{(GA\kappa I + EIA)^2\rho^2\omega^4 - 4(EIGA\kappa)(\rho A\omega^2)(\rho I\omega^2 - GA\kappa)}}{2EIGA\kappa}} \tag{58}$$

$$k_2 = -k_1 \tag{59}$$

$$k_3 = \sqrt{\frac{-(GA\kappa I + EIA)\rho\omega^2 - \sqrt{(GA\kappa I + EIA)^2 \rho^2\omega^4 - 4(EIGA\kappa)(\rho A\omega^2)(\rho I\omega^2 - GA\kappa)}}{2EIGA\kappa}} \tag{60}$$

$$k_4 = -k_3 \tag{61}$$

Finally, the transverse displacement $W(x,t)$ and angular displacement $\Theta(x,t)$ are given by

$$W(x,t) = \alpha_1 e^{k_1 x} + \alpha_2 e^{k_2 x} + \alpha_3 e^{k_3 x} + \alpha_4 e^{k_4 x} \tag{62}$$

$$\Theta(x,t) = \beta_1 e^{k_1 x} + \beta_2 e^{k_2 x} + \beta_3 e^{k_3 x} + \beta_4 e^{k_4 x} \tag{63}$$

Where

$$\alpha_i = c_i \beta_i = \frac{k_i}{k_i^2 + \frac{\rho A\omega^2}{GA\kappa}} \beta_i \tag{64}$$

Similar to the conventional beam finite element, two nodal displacements per node (one transverse and angular displacement per node) and replace four wave coefficients,

$$\begin{bmatrix} W_1 \\ \Theta_1 \\ W_2 \\ \Theta_2 \end{bmatrix} = P \begin{bmatrix} \beta_1 \\ \beta_2 \\ \beta_3 \\ \beta_4 \end{bmatrix} = \begin{bmatrix} c_1 & c_2 & c_3 & c_4 \\ 1 & 1 & 1 & 1 \\ c_1 e^{k_1 l} & c_2 e^{k_2 l} & c_3 e^{k_3 l} & c_4 e^{k_4 l} \\ e^{k_1 l} & e^{k_2 l} & e^{k_3 l} & e^{k_4 l} \end{bmatrix} \begin{bmatrix} \beta_1 \\ \beta_2 \\ \beta_3 \\ \beta_4 \end{bmatrix} \tag{65}$$

where l is the length of the element. Based on the Timoshenko beam theory, the shear force and bending moment are given by

$$V = GA\kappa\left(\frac{\partial w}{dx} - \theta\right) \tag{66}$$

$$M = EI\frac{\partial \theta}{\partial x} \tag{67}$$

Then we can define the elemental dynamic stiffness matrix K_e to link the nodal displacements and forces as shown below

$$\begin{bmatrix} V_1 \\ M_1 \\ V_2 \\ M_2 \end{bmatrix} = [K_e] \begin{bmatrix} W_1 \\ \Theta_1 \\ W_2 \\ \Theta_2 \end{bmatrix} \tag{68}$$

where

$$[K_e] = \begin{bmatrix} -GA\kappa(c_1k_1 - 1) & -GA\kappa(c_2k_2 - 1) & -GA\kappa(c_3k_3 - 1) & -GA\kappa(c_4k_4 - 1) \\ -EIk_1 & -EIk_2 & -EIk_3 & -EIk_4 \\ GA\kappa(c_1k_1 - 1)e^{k_1 l} & GA\kappa(c_2k_2 - 1)e^{k_2 l} & GA\kappa(c_3k_3 - 1)e^{k_3 l} & GA\kappa(c_4k_4 - 1)e^{k_4 l} \\ EIk_1 e^{k_1 l} & EIk_2 e^{k_2 l} & EIk_3 e^{k_3 l} & EIk_4 e^{k_4 l} \end{bmatrix} [P]^{-1} \tag{69}$$

3.2 Reduce PDE to ODE

Assuming harmonic response, the displacements u_0, w_0 and θ_i can be written in the following forms

$$u_0 = \bar{u}_0 e^{j\omega t} \tag{70}$$

$$w_0 = \bar{w}_0 e^{j\omega t} \tag{71}$$

$$\theta_i = \bar{\theta}_i e^{j\omega t} \tag{72}$$

Here $\bar{u}_0$, $\bar{w}_0$ and $\bar{\theta}_i$ are the amplitudes of u_0, w_0 and θ_i where ω is the angular (or circular) frequency of excitation. Taking second derivatives of Eq. (70) - (72)

$$\ddot{u}_0 = -\omega^2 \bar{u}_0 e^{j\omega t} \tag{73}$$

$$\ddot{w}_0 = -\omega^2 \bar{w}_0 e^{j\omega t} \tag{74}$$

$$\ddot{\theta}_i = -\omega^2 \bar{\theta}_i e^{j\omega t} \tag{75}$$

and substituting into Eq. (36), and rearranging, we obtain the following formulation of axial equilibrium equation.

$$\left(\sum_{i=1}^{n}(EA)_i\right)\frac{d^2\overline{u}_0}{dx^2}-\sum_{i=1}^{n}\left[\left(\frac{1}{2}(EA)_i+\sum_{j=i+1}^{n}(EA)_j\right)h_i\right]\frac{d^2\overline{\theta}_i}{dx^2}=-\sum_{i=1}^{n}m_i\omega^2\overline{u}_0+\sum_{i=1}^{n}\left[\left(\frac{1}{2}m_i+\sum_{j=i+1}^{n}m_j\right)h_i\omega^2\right]\overline{\theta}_i \quad (76)$$

Assuming free vibration (i.e. $q=0$), and by substituting Eq. (74) and Eq. (75) into Eq.(37), and rearranging, we obtain the following formulation of the transverse equilibrium equation.

$$\sum_{i=1}^{n}(GA)_i\frac{d^2\overline{w}_0}{dx^2}=\sum_{i=1}^{n}(GA)_i\frac{d\overline{\theta}_i}{dx}-\sum_{i=1}^{n}\left(m_i\omega^2\right)\overline{w}_0 \quad (77)$$

Equation obtained from substituting Eq. (73) and Eq. (75) into Eq. (38) can be expressed as

$$A=B \quad (78)$$

where

$$A=\sum_{i=1}^{n}\left[\begin{array}{r}\left[-\frac{h_i}{2}(EA)_i-h_i\left(\sum_{j=i+1}^{n}(EA)_j\right)\right]\frac{d^2\overline{u}_0}{dx^2}+(EI^c)_i\frac{d^2\overline{\theta}_i}{dx^2}+\frac{h_i}{2}(EA)_i\sum_{j=1}^{i-1}\left(h_j\frac{d^2\overline{\theta}_j}{dx^2}\right)+\frac{h_i^2}{4}(EA)_i\frac{d^2\overline{\theta}_i}{dx^2}\\ +h_i\left(\sum_{j=i+1}^{n}(EA)_j\sum_{k=1}^{j-1}h_k\frac{d^2\overline{\theta}_k}{dx^2}\right)+h_i\left(\sum_{j=i+1}^{n}(EA)_j\frac{h_j}{2}\frac{d^2\overline{\theta}_j}{dx^2}\right)\end{array}\right] \quad (79)$$

$$B=\sum_{i=1}^{n}\left[\begin{array}{r}\left[\frac{h_i}{2}m_i\omega^2+h_i\sum_{j=i+1}^{n}m_j\omega^2\right]\overline{u}_0-(GA)_i\frac{d\overline{w}_0}{dx}+\left((GA)_i-J_i\omega^2-\frac{h_i^2}{4}m_i\omega^2\right)\overline{\theta}_i-\left(\frac{h_i}{2}m_i\omega^2\sum_{j=1}^{i-1}h_j\overline{\theta}_j\right)\\ -h_i\left(\sum_{j=i+1}^{n}m_j\omega^2\sum_{k=1}^{j-1}h_k\overline{\theta}_k\right)-\frac{h_i}{2}\left(\sum_{j=i+1}^{n}m_j\omega^2h_j\overline{\theta}_j\right)\end{array}\right] \quad (80)$$

3.3 Develop State-Space Model

Providing closed-form solutions of Eqs. (76) - (78) is extremely difficult for high number of layers. An analytical solution expression is extremely lengthy even for a three layered sandwich beam. However, above equations are a set of second order ordinary differential equations. There is a standard matrix solution format for these coupled ordinary differential equations when the state space model is applied. However, we need to numerically determine some associated parameters, which lead to semi-analytical solution. First we need to define the state vector Z, which is given by

$$Z = \left[\bar{u}_0 \quad \bar{w}_0 \quad \bar{\theta}_1 \quad \ldots \quad \bar{\theta}_n \quad \frac{d\bar{u}_0}{dx} \quad \frac{d\bar{w}_0}{dx} \quad \frac{d\bar{\theta}_1}{dx} \quad \ldots \quad \frac{d\bar{\theta}_n}{dx} \right]^T \tag{81}$$

Then, above equation can be written in terms of state vector Z.

$$Y\frac{dZ}{dx} = XZ \tag{82}$$

Where X and Y are both $2n+4 \times 2n+4$ matrices, and they are constructed as follows

$$X = \left[\begin{array}{ccccc|cccc} & & [0]_{n+2\times n+2} & & & & & [I]_{n+2\times n+2} & & \\ \hline X_{n+3,1} & 0 & X_{n+3,k} & \cdots & X_{n+3,n+2} & 0 & 0 & 0 & \cdots & 0 \\ 0 & X_{n+4,2} & 0 & \cdots & 0 & 0 & 0 & X_{n+4,k} & \cdots & X_{n+4,2n+4} \\ X_{n+5,1} & 0 & & & & 0 & X_{(n+5),(n+4)} & 0 & 0 & 0 \\ \vdots & \vdots & & [X_{sub}]_{n\times n} & & \vdots & \vdots & 0 & 0 & 0 \\ X_{2n+4,1} & 0 & & & & 0 & X_{(2n+4),(n+4)} & 0 & 0 & 0 \end{array}\right]_{2n+4\times 2n+4} \tag{83}$$

The coefficients of Eq. (83) are given by

$$X_{n+3,1} = -\sum_{i=1}^{n} m_i \omega^2 \tag{84}$$

$$X_{n+3,k} = \sum_{i=1}^{n}\left(\frac{1}{2}m_i + \sum_{j=i+1}^{n} m_j\right)h_i\omega^2 \quad \text{where } k = 3\ldots(n+2) \tag{85}$$

$$X_{n+4,2} = -\sum_{i=1}^{n} m_i\omega^2 \tag{86}$$

$$X_{n+4,k} = (GA)_i \quad \text{where} i = 1\ldots n \text{ and } k = (n+5)\ldots(2n+4) \tag{87}$$

$$X_{k,1} = \sum_{i=1}^{n}\left(\frac{h_i}{2}m_i\omega^2 + \sum_{j=i+1}^{n} h_i m_j\omega^2\right) \quad \text{where } k = (n+5)\ldots(2n+4) \tag{88}$$

$$X_{k,(n+4)} = -(GA)_i \quad \text{where} i = 1\ldots n \text{ and } k = (n+5)\ldots(2n+4) \tag{89}$$

$$[X_{sub}]_{i,j} = \sum_{i=1}^{n}\left[\begin{array}{r}\displaystyle\sum_{j=i}^{n}\left((GA)_i - J_i\omega^2 - \frac{h_i^{\,2}}{4}m_i\omega^2\right) - \sum_{j=1}^{i-1}\left(\frac{h_i}{2}m_i\omega^2 h_j\right) \\ \displaystyle - \sum_{j=i+1}^{n}\left(\frac{h_i}{2}m_j\omega^2 h_j\right) - \sum_{k=i+1}^{n}\sum_{j=1}^{k}\left(h_i h_j m_k\omega^2\right)\end{array}\right] \tag{90}$$

where i is the row number, and j is the column number of the X_{sub} sub matrix. Y in Eq. (82) is also a $2n+4 \times 2n+4$ matrix, and it is constructed as follows

$$Y = \left[\begin{array}{c|cccccc} [I]_{n+2\times n+2} & [0]_{n+2\times n+2} & & & & & \\ \hline & Y_{n+3,n+3} & 0 & Y_{n+3,k} & \cdots & Y_{n+3,2n+4} \\ & 0 & Y_{n+4,n+4} & 0 & \cdots & 0 \\ [0]_{n+2\times n+2} & Y_{n+5,n+3} & 0 & & & \\ & \vdots & \vdots & & [Y_{sub}]_{n\times n} & \\ & Y_{2n+4,n+3} & 0 & & & \end{array}\right]_{2n+4\times 2n+4} \tag{91}$$

The coefficients of Eq. (91) are given by

$$Y_{n+3,n+3} = \sum_{i=1}^{n} (EA)_i \tag{92}$$

$$Y_{n+3,k} = -\sum_{i=1}^{n}\left(\frac{1}{2}(EA)_i + \sum_{j=i+1}^{n}(EA)_j\right)h_i \tag{93}$$

where $i = 1\ldots n$ and $k = (n+5)\ldots(2n+4)$

$$Y_{n+4,n+4} = \sum_{i=1}^{n} (GA)_i \tag{94}$$

$$Y_{k,(n+3)} = -\sum_{i=1}^{n}\left[\frac{h_i}{2}(EA)_i + \sum_{j=i+1}^{n} h_i (EA)_j\right] \tag{95}$$

where $i = 1\ldots n$ and $k = (n+5)\ldots(2n+4)$

$$[Y_{sub}]_{i,j} = \sum_{i=1}^{n}\left[\sum_{j=i}^{n}\left((EI)_i + \frac{h_i^{\,2}}{4}(EA)_i\right) + \sum_{j=1}^{i-1}\left(\frac{h_i}{2}(EA)_i h_j\right) + \sum_{j=i+1}^{n}\sum_{k=1}^{j-1} h_i (EA)_j h_k + \sum_{j=i+1}^{n}\frac{h_i h_j}{2}(EA)_j\right] \tag{96}$$

where i is the row number, and j is the column number of the Y_{sub} sub matrix. Now the governing equations are simple second order ODE. This is an eigenvalues problem and, the solution of vector Z is given by

$$Z = Z_0^{\left(Y^{-1}X\right)x} = Z_0^{Ax} \tag{97}$$

Eigenvalues of the matrix A in Eq. (97) can be calculated numerically to determine wave numbers. The corresponding eigenvectors define the ratio of each component in the state vector Z.

3.4 Develop Dynamic Stiffness Matrix

Development of dynamic stiffness matrix starts with the definition of nodal displacement vector and the corresponding nodal force vector. Figure 3 shows a single spectral finite element of a multi-layered beam. Then, nodal displacements are used to solve for unknown coefficients in the displacement solutions. Then, we can relate the nodal force vector with the nodal displacement using a matrix, which is identified as dynamic stiffness matrix as shown below.

$$\hat{F} = D(\omega)\hat{u} \tag{98}$$

For the multi-layered beam, Eq. (98) can be expressed in the following form

$$\begin{Bmatrix} N_1 \\ V_1 \\ M_{1L} \\ \vdots \\ M_{nL} \\ N_2 \\ V_2 \\ M_{2R} \\ \vdots \\ M_{nR} \end{Bmatrix} = [D] \begin{Bmatrix} U_1 \\ W_1 \\ \theta_{1L} \\ \vdots \\ \theta_{nL} \\ U_2 \\ W_2 \\ \theta_{2R} \\ \vdots \\ \theta_{nR} \end{Bmatrix} \tag{99}$$

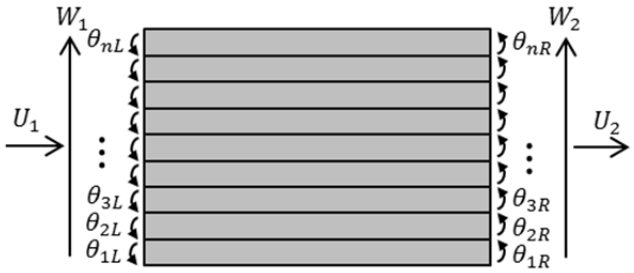

(a) Nodal Displacement Components

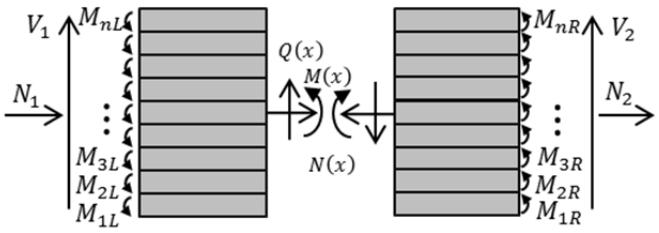

(b) Nodal Force Components

Figure 3. Spectral Finite Element of a Multi-Layered Beam.

3.5 Assemble Dynamic Stiffness Matrix

Following the same fashion as the conventional finite element approach, the global dynamic stiffness matrix can be assembled by using individual element dynamic stiffness matrices. Each element has two end nodes and adjacent elements share a common node. By applying appropriate boundary conditions, we can conduct dynamic analysis and predict the response of a multi-layered beam. For the free vibration, instead of solving the eigenvalue problem as practiced in the conventional finite element method, we find the roots of the determinant of the final dynamic stiffness matrix. On the other hand, for the forced vibration, we first need to conduct the FFT to determine force components under each frequency. Then we can solve the displacements accordingly in the frequency domain. Finally, the time domain displacement solutions can be realized by conducting inverse FFT. This process is shown in Figure 4.

In this thesis, the time domain data is obtained by evaluating the global dynamic stiffness matrix numerically using MATLAB. First elemental dynamic stiffness matrix is calculated, and global dynamic stiffness matrix is formed based on the number of elements used in the problem definition. Then FFT (Fast Fourier Transform) function is used to convert time domain input signal into frequency domain. The displacements are then solved in frequency domain and then time domain displacement is obtained by conducting IFFT (Inverse Fast Fourier Transform) function. A MATLAB program is coded to carry out these calculations, and the results are presented in the following chapter.

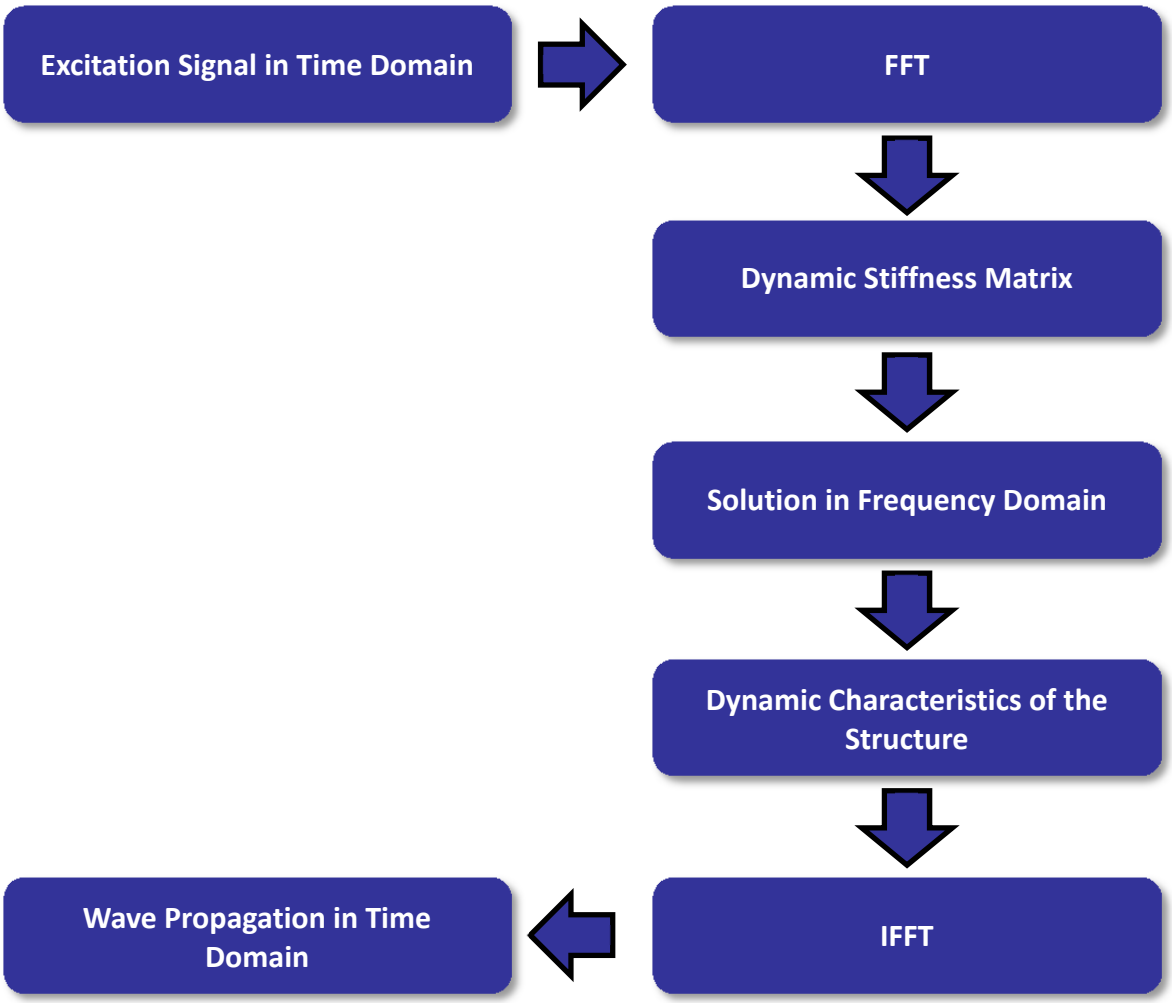

Figure 4. SFEM Formulation Steps

CHAPTER 4

RESULTS

Validation of the developed spectral finite element model has been carried out by calculating free vibration frequencies of two and three layer beams, and comparing with the results available in the literature. In addition, Frequency Response Function (FRF) of each beam is compared with FEM (Nastran) results to show the convergence with higher number of elements. After the model is verified, a frequency sensitivity study has been carried out to determine if modal based damage detection is a feasible approach in damage detection. Then, wave propagation response is determined for a similar two layer beam under a high frequency impulse excitation. Damaged cases are simulated by introducing a thickness reduction in the top layer, and corresponding wave propagation responses can be determined under different damage levels.

4.1 Modal Analysis

4.1.1 2-Layer Beam

The first example considers the free vibration response of a two layer cantilever beam, with 5mm aluminum and a 0.75 mm steel layer as it is shown in Figure 5. The overall length of the beam is 0.3m, with 20mm width. The geometric and material properties are also given in Table 1.

Table 1. Geometric and material properties of the two-layer beam.

	Layer 1	Layer 2
L (m)	0.300	0.300
b (m)	0.020	0.020
h (m)	0.005	0.00075
E (GPa)	70	200
ρ (kg/m^3)	2700	7850

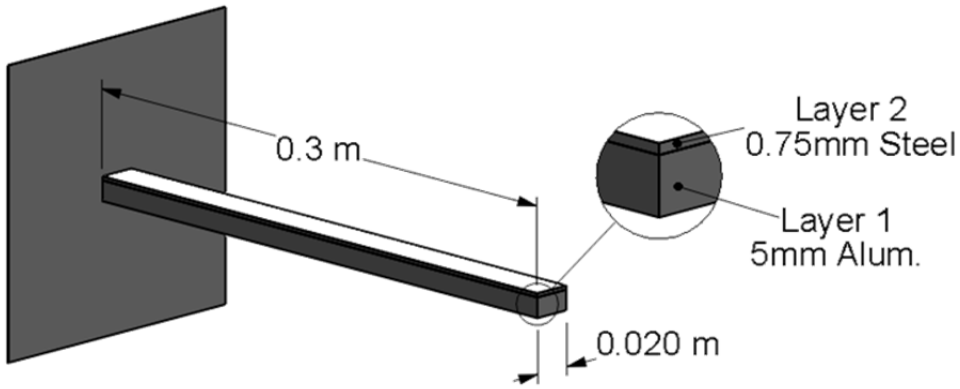

Figure 5. Two-layer beam

The first five modal frequencies are calculated, and compared with Lee's results in Table 2. It is clearly shown that the SFEM values are very close to literature results, indicating the validity of the model.

Table 2. Modal Frequencies of the two-layer beam. (Hz)

Mode	FEM Ref. [3]		SFEM Ref. [3]	SFEM
	N=40	N=100	N=1	N=1
1st	56.5551	56.554	56.5538	56.534
2nd	354.378	354.330	354.321	353.45
3rd	992.054	991.738	991.686	985.94
4th	1943.42	1942.28	1942.06	1921.5
5th	3211.32	3208.29	3207.71	3154.2
10th	11429.25	11392.55	11385.70	10796.20

In addition, the beam is modeled using QUAD4 plate elements, and the free vibration characteristic of the beam is analyzed in NASTRAN. The analysis has been repeated with different number of elements, and the result, frequency response function (FRF), is shown in Figure 6. As it can clearly be seen from the figure, for the first two-three low frequencies, relatively few numbers of elements provide good accuracy, whereas with the increasing frequency, higher number of elements is needed in FEM. In this case, as many as 500 elements are needed to provide a comparable accuracy at the 5th mode, which introduces a significant

computational cost to the analysis. On the other hand, a single element is sufficient to model a uniform section of a beam, resulting in a substantial computational cost.

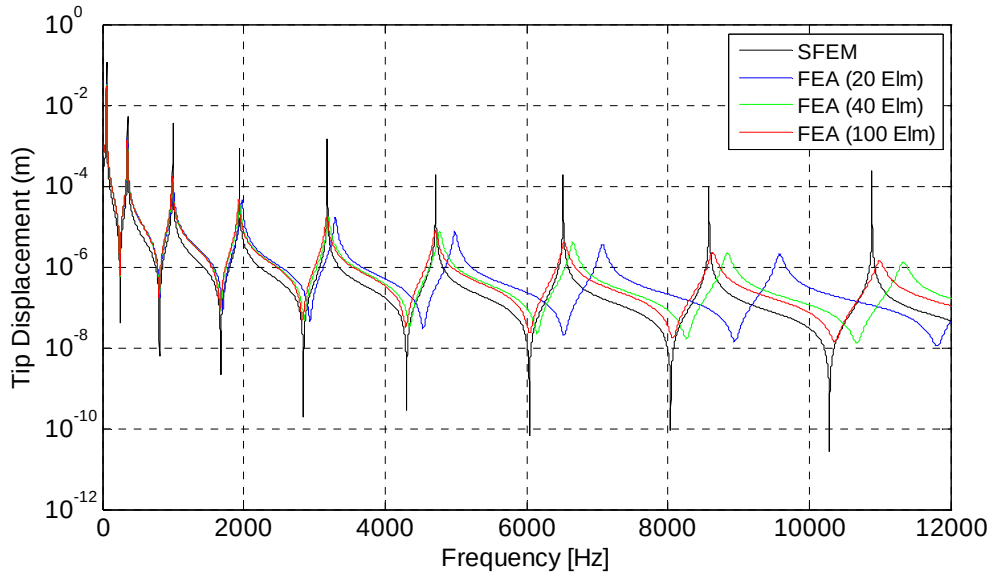

Figure 6. Frequency Response Function (FRF) of the Two-Layered beam

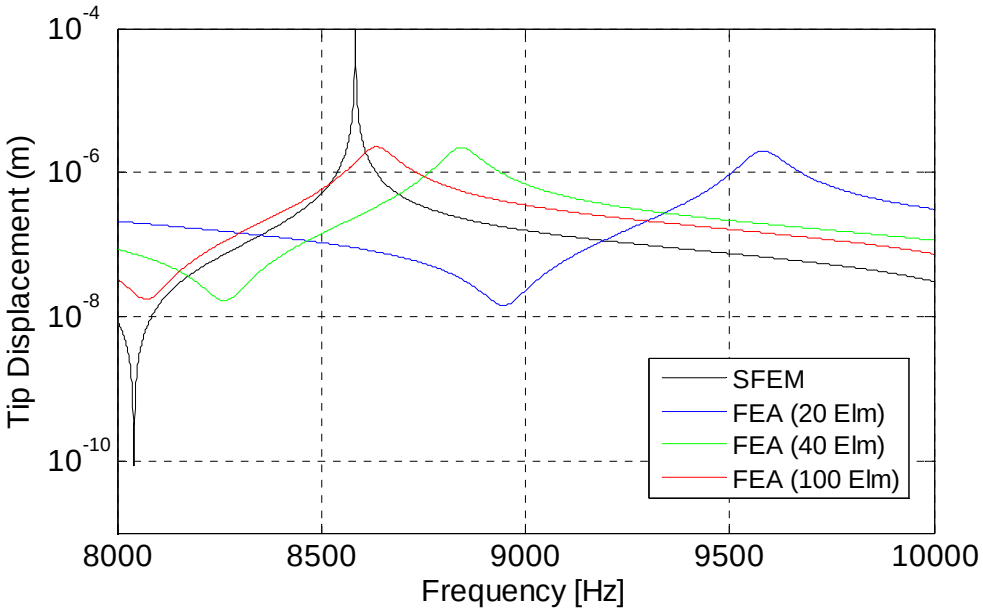

Figure 7. FRF of the Two-Layered Beam: 8000-10000 Hz

4.1.2 3-Layer Beam

The second example considers the free vibration response of a three-layer sandwich beam Ref [27] as shown in Figure 8. The beam has an overall length of 0.5m, and composed of 15mm steel, a 20mm lead and a 10mm steel top layer. The geometric and material properties are listed in Table 3.

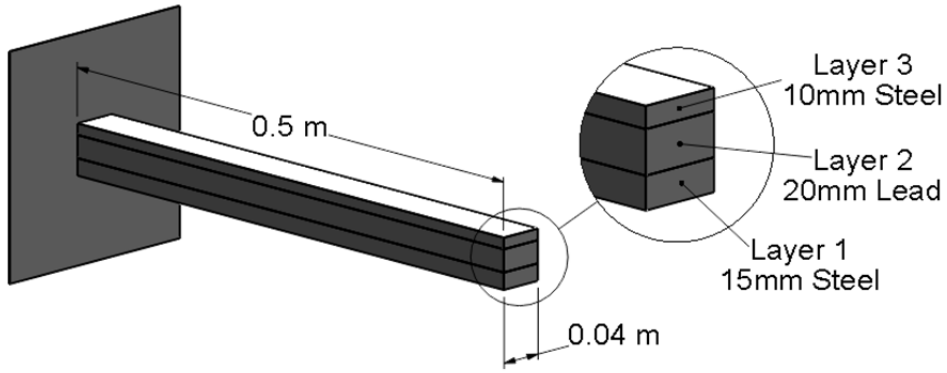

Figure 8. Three-layer beam.

Table 3. Geometric and material properties of the three-layer beam.

	Layer 1	Layer 2	Layer
L (m)	0.5	0.5	0.5
b (m)	0.04	0.04	0.04
h (m)	0.015	0.02	0.01
E (GPa)	210	16	210
G (GPa)	80	5.5	80
ρ (kg/m^3)	7850	11100	7850
κ	2/3	2/3	2/3

The first four modes are calculated, and compared with the results from Ref [9]. The results, again, are very close to literature results, indicating the validity of the model.

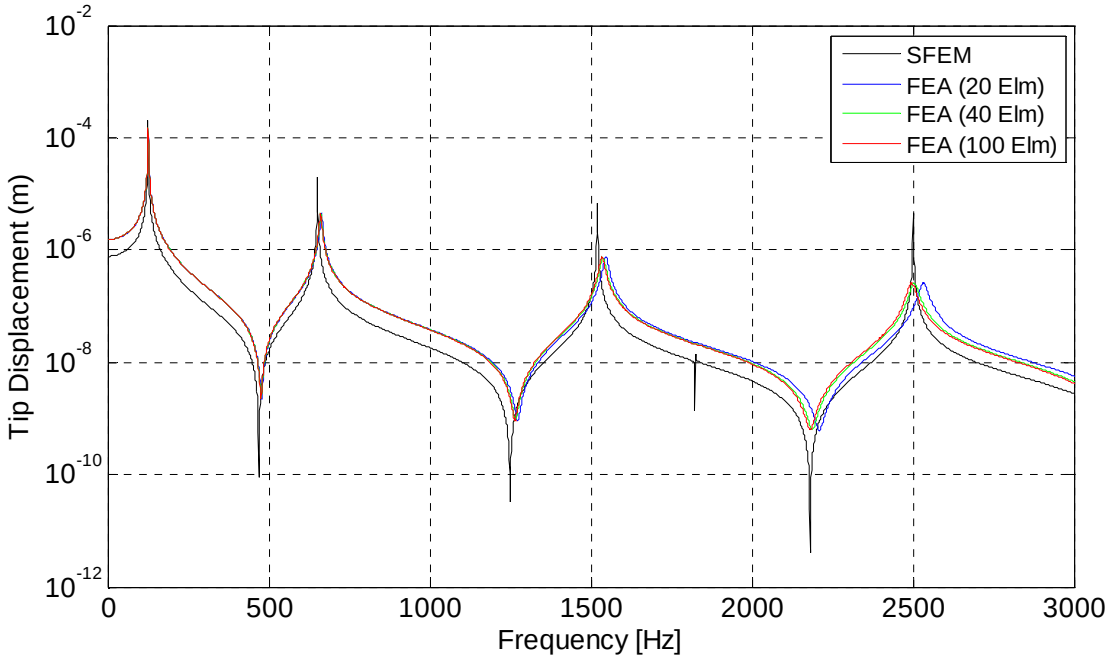

Figure 9. Frequency Response Function (FRF) of the three-layered beam

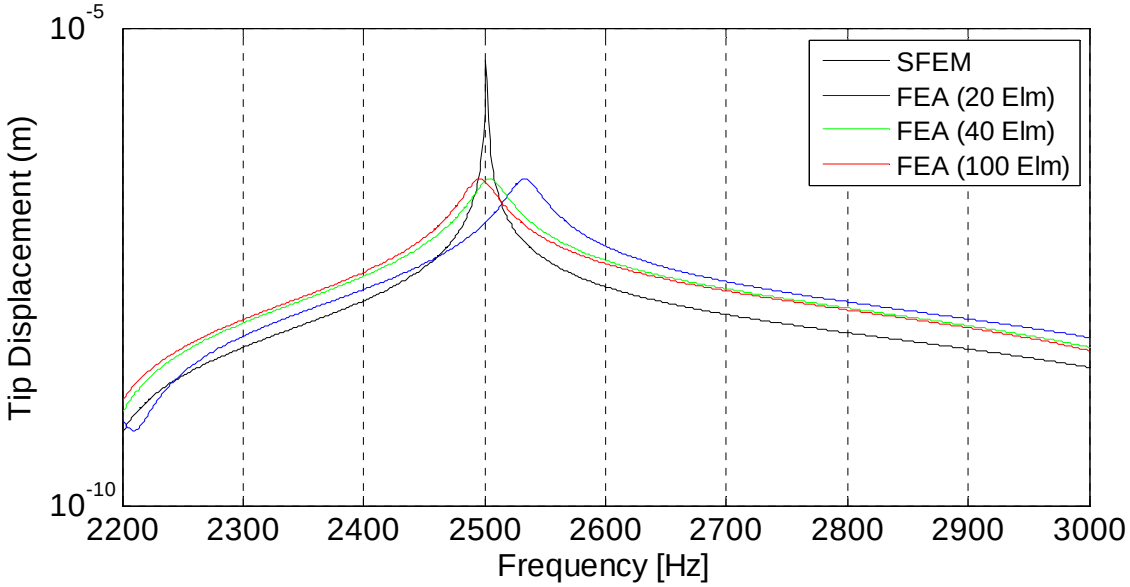

Figure 10. FRF of the Three-Layered Beam (2200-3000 Hz)

Table 4. Modal Frequencies of the three-layer beam. (Hz)

Mode	Ref. [9]	SFEM	% Difference
1st	123.56	123.29	0.20
2nd	611.33	611.52	0.03
3rd	1393.1	1396.6	0.25
4th	1823.79	1823.8	~ 0

As it was carried out in the previous example, FRF with different element sizes is investigated to see the convergence with increasing number of elements. The result is shown in Figure 9, and it can clearly be seen that with the increasing number of elements, the response converges to the SFEM, which is the exact method. However, with the increasing number of elements, more computation time is required, whereas a single element is sufficient in SFEM, which offers a much faster and accurate solution.

4.1.3 Frequency Sensitivity Study

Cracks or other defects are known to cause a change in vibration characteristics in a structural element by affecting its stiffness and damping properties. Thus, provided that the natural frequencies are known for a structure in undamaged state, the damage in the structure can be detected by tracking the changes in natural frequencies. This study analyzes a cantilevered beam with a damage modeled in the form of a varying depth thickness in the middle of the beam, to investigate if modal based damage detection is a feasible approach in detecting the damage in the structure.

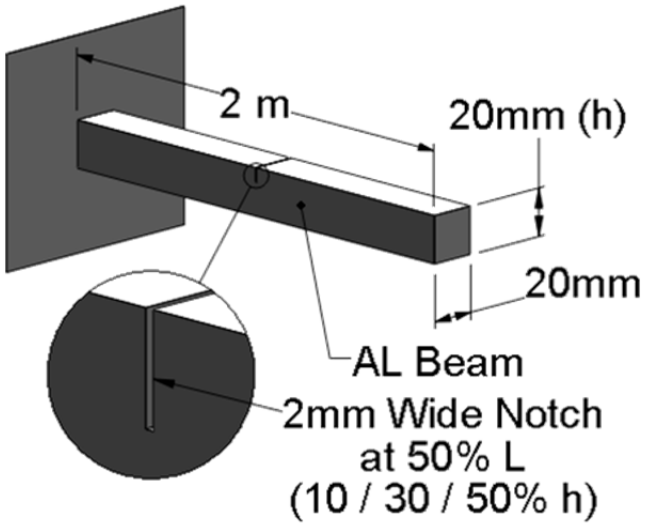

Figure 11. Damaged beam for Frequency Sensitivity Study

The beam used in the analysis has a 20mm square cross-section, with an overall length of 2m. The 2mm notch simulating the damage is located in the middle of the beam. The analysis has been carried out for a wide frequency range with 10%, 30%, and 50% notch depth, and the calculated natural frequencies are compared with the undamaged base frequency. The results are tabulated in Table 5. It should be noted that in some modes, the notch is at the location of a node in the mode shape, resulting in 0% difference, as it is shown in Figure 12 for the third mode as an example. These modes are removed from the table for clarity.

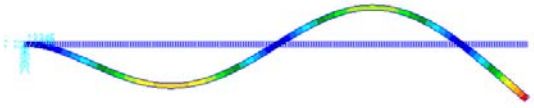

Figure 12. 3rd Mode Shape in Frequency Sensitivity Example

Table 5. Frequency Sensitivity Study

Mode	Undamaged (rad/s)	Notch Depth (% of Layer Height)					
		10%		30%		50%	
		Freq.	%	Freq.	%	Freq.	%
1st	25.838	25.836	0.01%	25.830	0.03%	25.799	0.15%
2nd	161.850	161.805	0.03%	161.580	0.17%	160.795	0.65%
4th	886.407	886.167	0.03%	884.990	0.16%	880.824	0.63%
6th	2181.936	2181.351	0.03%	2178.490	0.16%	2168.401	0.62%
8th	4039.261	4038.201	0.03%	4033.458	0.14%	4024.097	0.38%
10th	6443.994	6442.303	0.03%	6434.101	0.15%	6406.042	0.59%
12nd	9378.256	9375.830	0.03%	9364.049	0.15%	9323.571	0.58%
14th	12821.261	12818.002	0.03%	12802.417	0.15%	12752.793	0.53%
16th	16749.916	16745.728	0.03%	16725.484	0.15%	16657.313	0.55%
18th	21139.452	21134.281	0.02%	21109.679	0.14%	21033.420	0.50%
20th	25964.003	25957.771	0.02%	25927.564	0.14%	25825.099	0.53%
22nd	31197.153	31189.850	0.02%	31154.997	0.14%	31042.997	0.49%
24th	36812.434	36804.063	0.02%	36765.144	0.13%	36660.419	0.41%

It is noticeable that the changes in natural frequencies become more intensive with the growth of the crack in the beam. However, the effect of the crack on the natural frequencies is very small, less than 1% even in 50% damage case. Although there are some frequency variations in higher modes, it is very challenging to excite the structure at higher modes and obtain accurate data in an experiment. Therefore, it can be concluded that modal frequency based damage detection is not a feasible damage detection scheme, and a more feasible, robust and easier to implement way should be investigated.

4.2 Wave Propagation Response

4.2.1 Single Layer Beam Verification

In this section, the wave propagation response is investigated for a single layer cantilevered beam under a tip excitation force, and compared with conventional FEM results. Damage is simulated by a thickness reduction in the top layer, located at the middle of the beam. In this case, the thickness reduction is taken as 50%, and the tip displacement result is compared with Nastran prediction.

The beam used in the study has a 5mm by 2mm cross section with 1m overall length. The length of the notch, which represents the damage in the beam, is taken as 0.1% of the length of the beam as it is shown in Figure 13. As it was stated before, SFEM allows us to use a single element in the uniform section of the beam, therefore requiring only three elements to model the entire beam. The first element defines the first section, which starts from fixed end and ends at the damaged element, the second element defines the damaged section, and the third element defines the section from damaged element to the free end of the beam.

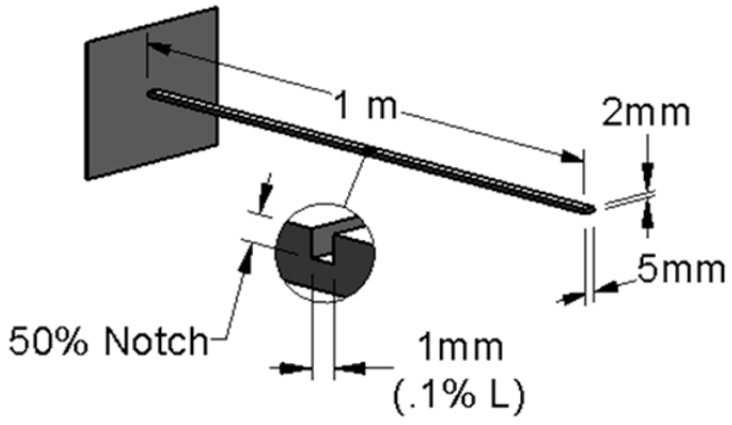

Figure 13. Single Layer Beam for Wave Propagation Response

The tip excitation force is a modulated 5-cycle 50 KHz sine burst by Hanning window, with duration of 0.1ms, as it is shown in Figure 14.

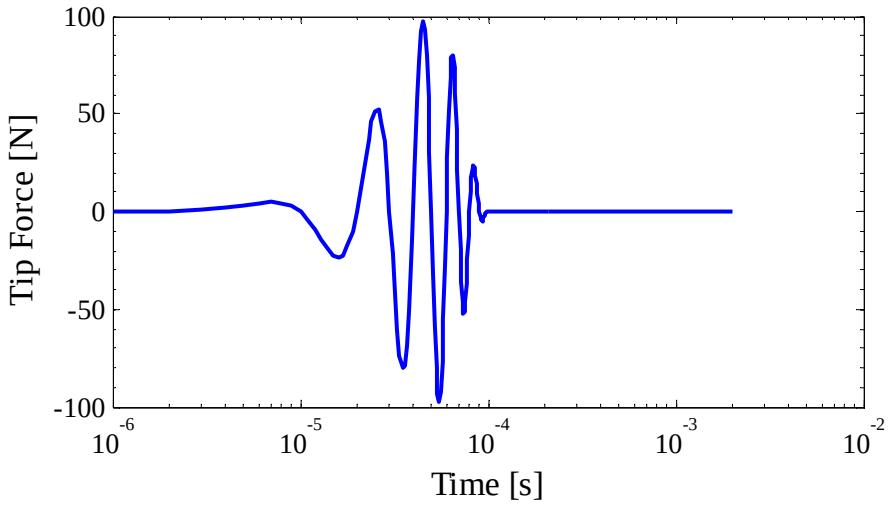

Figure 14. Waveform of Tip Force at 50KHz Sine Burst

In addition, in order to obtain relatively good results using conventional FEM method, significant amount of elements need to be used in the analysis. In this case 200 elements used over the length of the beam in Nastran analysis. The comparison between two approaches is given in Figure 15. The number of elements used in SFEM affects the analysis time significantly, yielding accurate results in a fraction of a time compared with classical FEM.

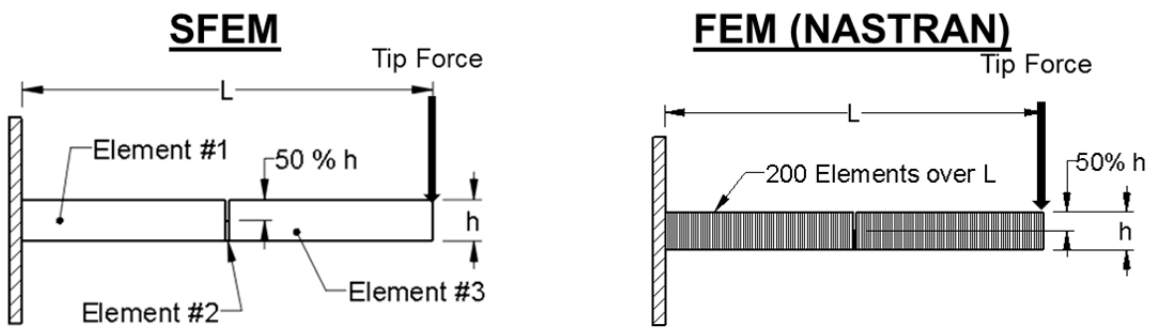

(a) **(b)**

Figure 15. SFEM & FEM Modeling Comparison

The analysis has been carried out, and the tip displacement data obtained from SFEM and FEM are shown in Figure 16.

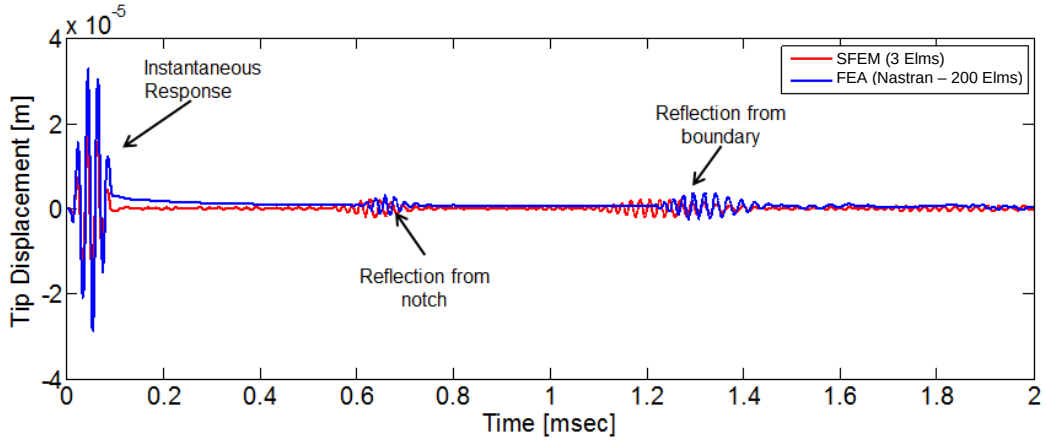

Figure 16. SFEM & FEM Wave Propagation Comparison

As it can be seen from the figure, the results obtained from both methods are similar. It is noticeable that there are three responses in the plot. The first response represents the excitation signal, i.e. instantaneous response. The wave travels over the length of the beam, and reflects

back from the notch, which is clearly visible on the timeline. The reflection from the boundary, i.e. fixed end of the beam, is also visible in the figure. Based on this comparison, we can obtain several conclusions, which are stated below.

First, it is possible to see that the amplitude of the reflection from the notch is less than the reflection from boundary. This is because the damaged element has 50% of the beam height, and the amplitude gives an insight about the extent of the damage. With the increasing damage, the amplitude from the notch will be higher. It is also clearly noticeable that the reflection from the notch is located in the middle of the timeline, between instantaneous response and the reflection from boundary. Based on this information, it can be concluded that the damage is located in the middle of the beam, which in fact is how the problem is defined.

The difference between two different methods both in terms of amplitude and timing of the tip response can easily be seen in the plot. It should be noted that the problem is modeled using a single layer “Laminated Composite” in Nastran. Although the plate offset is set to zero, to match the surface representing the beam with the bottom layer as it is defined in the developed SFEM, the difference is still visible. It is specified in Nastran manual that Classical Laminated Plate Theory is used in the analysis, which ignores any warping effects and it is less accurate compared with the developed SFEM. The difference in the kinematics between two approaches, results in a difference in the tip response of the beam.

Although both methods do not match closely, and a difference between two different tip response plots is observed, which indicates that the model gives accurate results of wave response.

4.2.2 Two Layer Beam Wave Propagation

Now that the model has been verified for modal analysis, as well as wave propagation characteristics for a single layer case using conventional FEM, the effect of different level of damage in the response will be investigated. A two-layer cantilever beam shown in Figure 17 will be used. For this case, damage is introduced by placing a notch in the middle of the beam. The thickness reduction at the notch is assumed to be 10%, 30% and 50% of the height of the top layer. The length of the beam is 1.5m, and it has a rectangular cross section (0.05 X 0.01 X 0.008 m, W X H1 X H2). The first layer is 10mm aluminum, and the second layer is an 8mm steel with 50mm width. The length of the notch is again assumed to be 0.1% of the length of the beam to be consistent with previous studies.

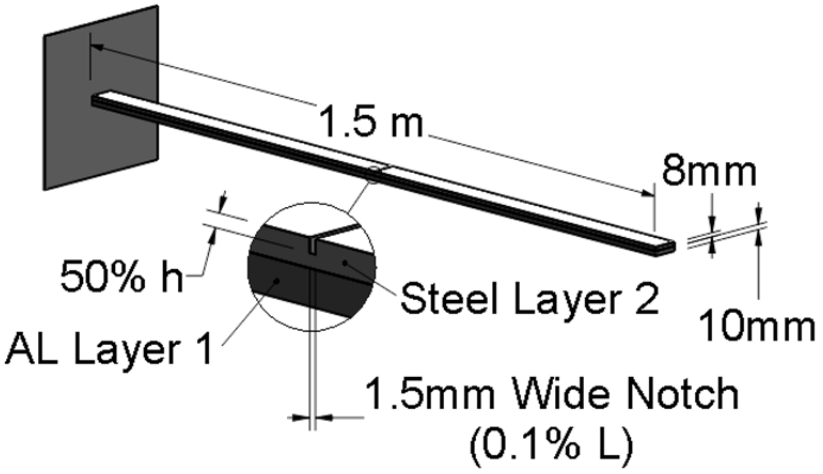

Figure 17. Two Layer Beam Wave Propagation

The beam contains a single damage over its length, as it is shown in Figure 15(a). As it was stated before, only any irregular sections of the beam needs to be modeled as an element in

SFEM, therefore only three elements are sufficient to model this beam. Two elements are used for undamaged regions at each end, and one element is used for the notch in the middle. The same tip excitation force, which is shown in Figure 14, is used in this analysis, and both baseline (no damage) and damaged cases (10%, 30%, and 50% thickness loss) were simulated with 0.5% damping. The tip displacement results are shown below for each damage case.

The undamaged baseline response of the beam is shown in Figure 18. Here both instantaneous response and the reflection from the boundary are clearly visible. With the introduction of damage in the beam, additional wave responses appear in the response curve. Figure 19 shows 10% notch depth case, and the waves reflected from the damaged element start to appear on the plot.

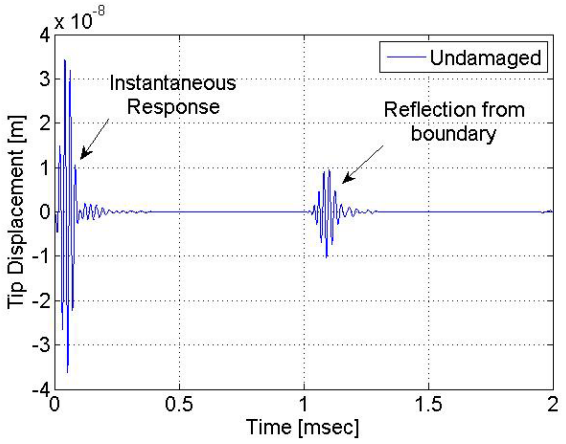

Figure 18. Undamaged beam response

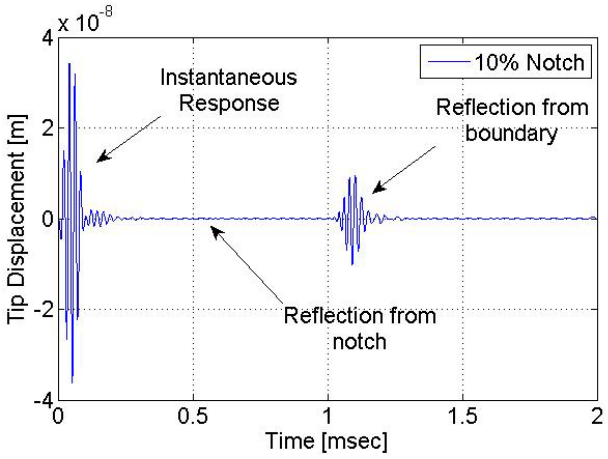

Figure 19. 10% Notch beam response

Figure 20 and Figure 21 show the increased notch depth at 30 and 50%. In these cases, the reflection waves become much more apparent, indicating the extent of the damage, i.e. the amplitude of the reflection waves increase with the increasing damage.

The location of the reflection waves on the plot is also an interest. When looked at closely, one can realize that the first reflection wave is located at the midpoint between the instantaneous response, and the reflection from boundary. The location of the reflection wave on the response is an indication of the location of the damage in the beam. Since the damage is placed in the middle of the beam, the first reflection wave appears between the instantaneous response and the reflection from boundary. This is clearly demonstrated in Figure 20 and Figure 21.

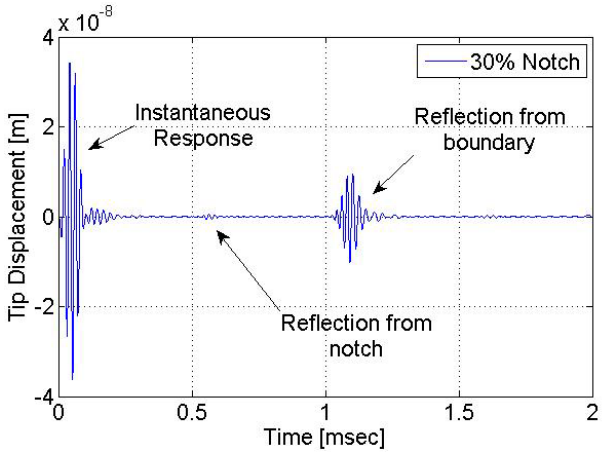

Figure 20. 30% Notch beam response

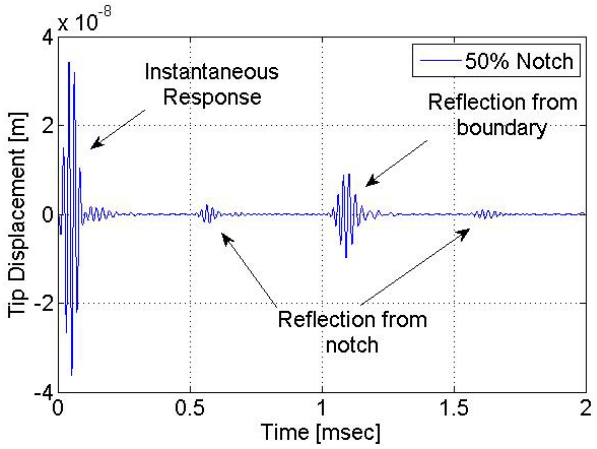

Figure 21. 50% Notch beam response

4.2.3 Multi-Layered SHM Application Example

In section 4.2.1, the developed SFEM has been verified by comparing the wave response with the response of a comparable finite element model to indicate the validity of the model. In section 4.2.2, the response of a two layered beam has been analyzed to identify and assess the extent of the damage located in the beam.

In this section, the wave propagation response of a multi-layered beam is investigated under a tip excitation force, similar to previous examples. The beam used in this case is 1.8m long, five layer cantilevered beam with different layer thicknesses of aluminum and steel. The first and fifth layers are 4mm aluminum, and the second and fourth layers are 6mm steel. The third (core) layer is selected to be thicker than other layers with 10mm aluminum. Damage is simulated similar to previous cases, but in this case, a layer loss is simulated by decreasing the top layer thickness by 99%. Finally, the damage length is taken as 1% of the beam length, which is equivalent to 18mm as it is shown in Figure 22.

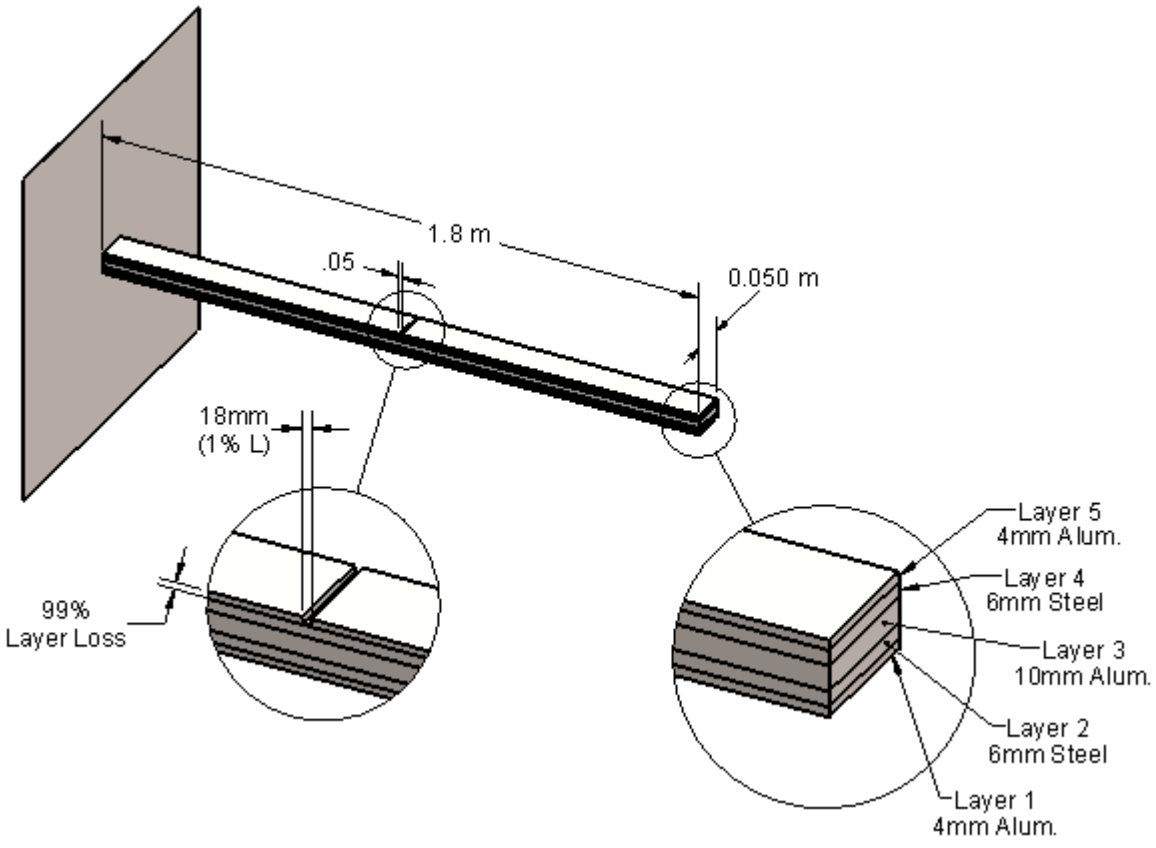

Figure 22. Multi-Layered Beam for Wave Propagation Response

The beam contains only a single damage over its length; therefore, as it has been stated before, three elements are sufficient to model this beam using SFEM. The same tip excitation force, which is shown in Figure 14 is used in this analysis.

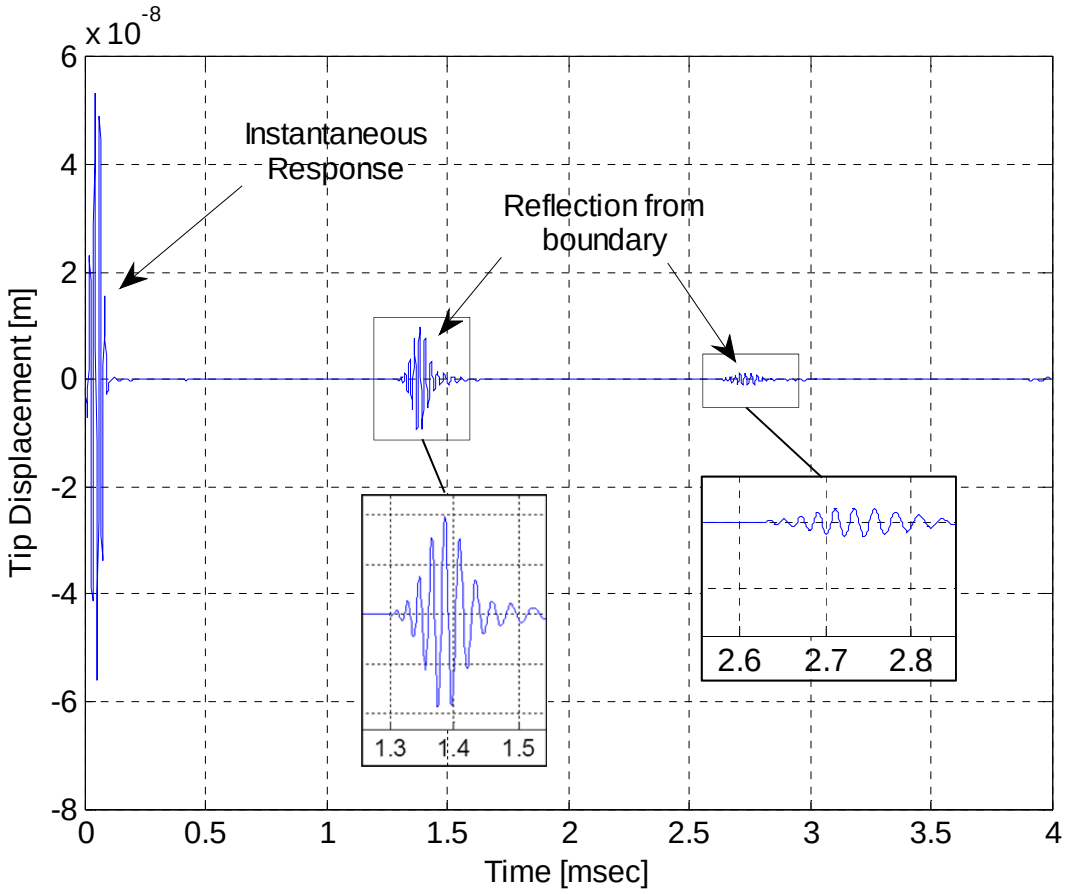

Figure 23. Undamaged Multi-Layer Beam Response

The analysis result is shown in Figure 23, in which both instantaneous response and the reflections from boundary are clearly visible. The horizontal timeline first shows the instantaneous response captured at the tip. The excitation signal travels along the length of the beam, and is reflected back from the fixed end, and captured as deflection at the tip as it is shown

in Figure 23. The two reflected signals correspond to approximately 1.3ms, and 2.6ms on the timeline. This figure will be used as the undamaged, baseline response of the beam, and will be compared with the damaged response.

Next, the damage in the top layer is introduced as decreased top layer thickness, and the analysis is re-run. Top layer thickness of the second element is reduced to its 1% original thickness, and the tip response is plotted as it is shown in Figure 24.

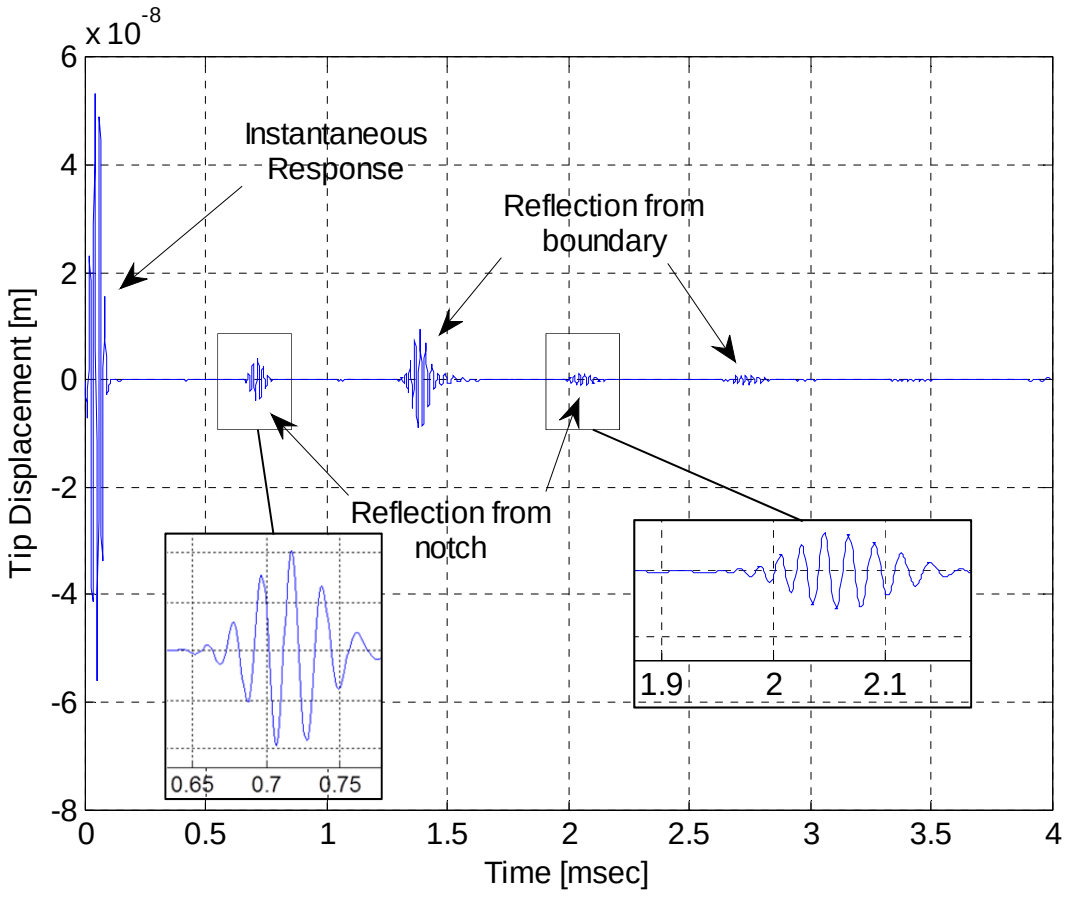

Figure 24. Damaged Multi-Layer Beam Response

The damaged plot shows the instantaneous response caught at the tip, as well as the reflections from the boundary, similar to undamaged case shown in Figure 23. A closer look reveals the reflections from the notch as expected. As it was indicated before, the reflections from boundary were obtained around 1.3ms and 2.6ms on the timeline. The reflections from the damaged element become visible around 0.65ms and right before 2ms (1.95ms to be more precise). These time values correspond to half values of the boundary reflection values, which indicate the damage location to be at half way between the tip, and the fixed end.

This example clearly shows that the model is capable of capturing wave propagation effectively for a multi-layered beam, and can be used as a SHM platform to effectively identify and assess the damage extend in a multi-layered beam structure.

4.3 Wave Based SHM Demonstration

In this section, the effect of different excitation signal frequency will be investigated. The same cantilevered beam used in Section 0 (5-layer multi-layered beam) will be analyzed using the tip excitation signal shown in Figure 14 at different frequencies, and tip displacement response will be plotted to compare with the previous case. It is expected that the higher frequency will be able to detect the damage and identify its extent better than lower frequencies. The following figure shows the tip response at 25 kHz tip excitation force for undamaged baseline response.

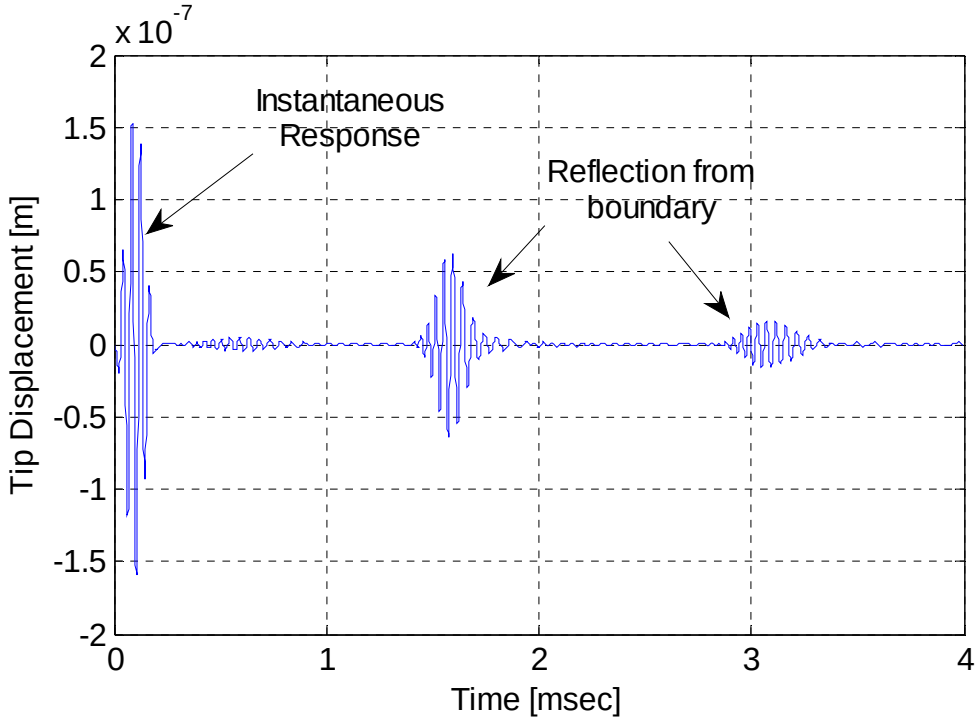

Figure 25. Undamaged Multi-Layer Beam Response (25 kHz)

The tip response is similar to previous case. Although there is some noise detected between the instantaneous response and the first reflection, both reflections, are clearly visible on the response. When the damage is introduced at the middle of the beam, and the analysis is rerun, the tip response plot shown in Figure 26, in which subtle difference from the undamaged case shown is obtained. Although a small amount of disturbance is seen and the damage is detected between the instantaneous response, and the first reflection, as well as between the two reflections, it is not clearly identified, and hard to detect. The same beam will be analyzed with a higher frequency tip force input, and the difference will be examined.

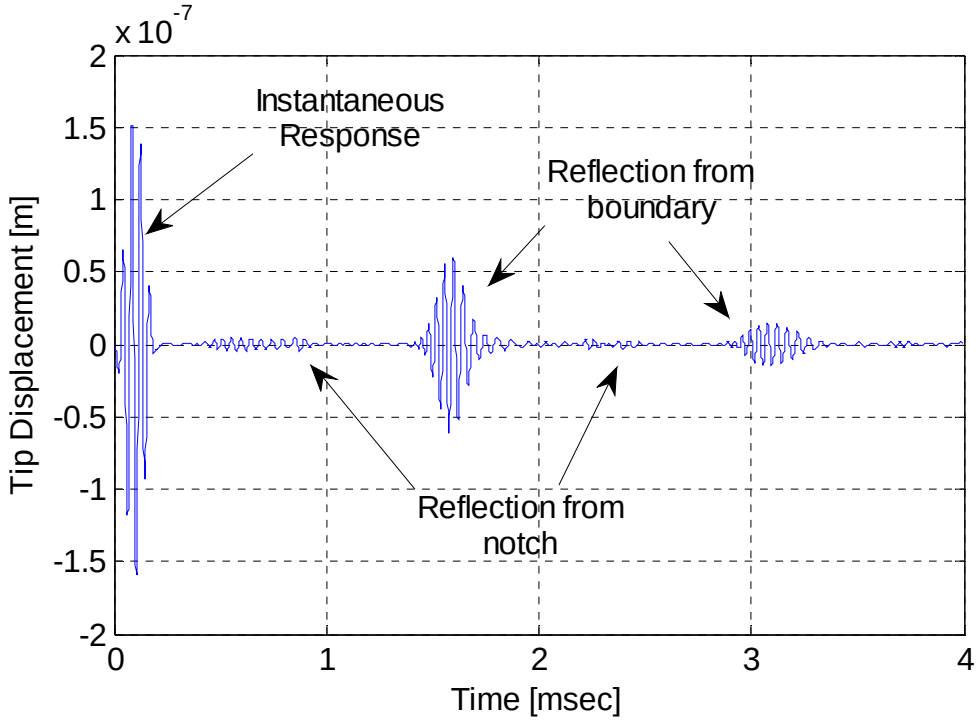

Figure 26. Damaged Multi-Layer Beam Response (25 kHz)

As a comparison of 25 kHz response with 50 kHz response, Figure 25 and Figure 23 and shown side by side in the following figure to illustrate the effect of increasing frequency in damage detection and identification. The difference between the two plots is more visible. The reflection from the damage becomes much more visible and distinctive with the increased frequency as it can clearly be seen from Figure 27. Damage detection and identification becomes easier with response data obtained at higher frequency. With the increasing frequency, damage can be detected and identified more easily.

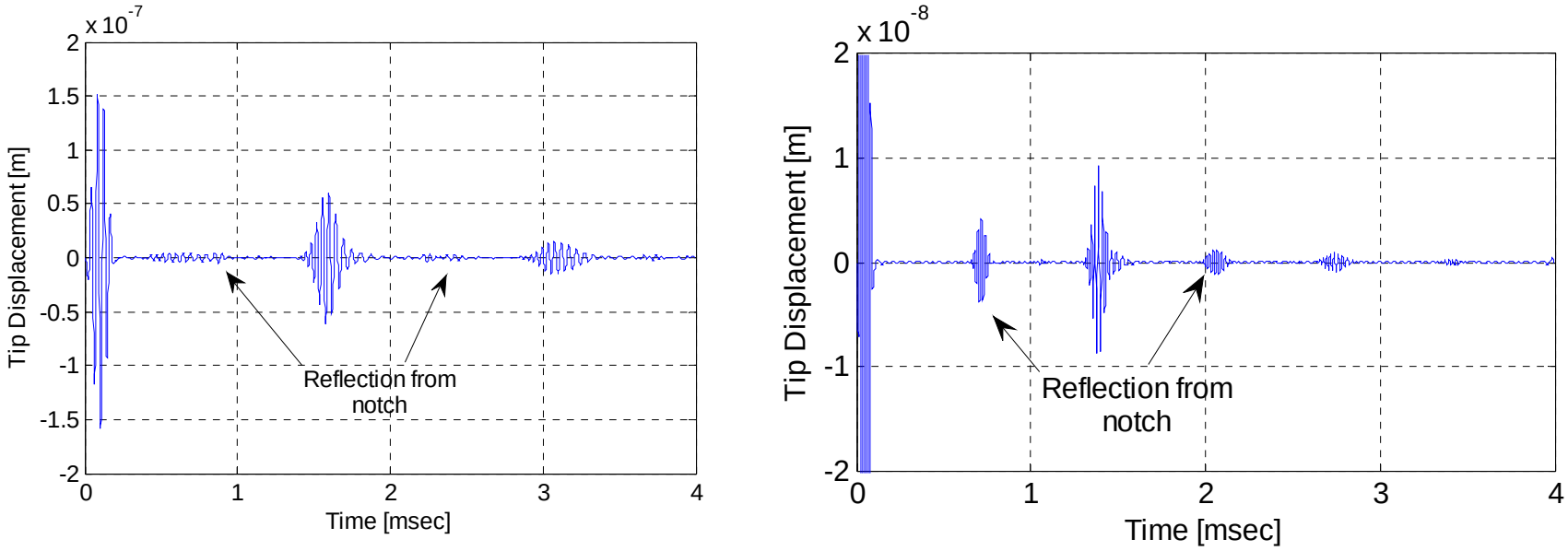

Figure 27. 25 kHz (left) vs. 50 kHz (right) Tip Response Comparison

CHAPTER 5

CONCLUSION

In this thesis, we first developed a higher order multi-layered beam model. For an *n*-layered beam, n+2 equations are obtained. Subsequently, the SFEM was formulated to obtain the wave propagation solutions accurately and efficiently. The developed model has been verified by comparing free vibration frequency results with several other models available in literature. In addition, the model has also been compared with a classical finite element model to show the effectiveness of the developed spectral finite element.

The damage detection capability of the model has first been analyzed through a frequency sensitivity study and the difference in modal frequency of a beam structure has been analyzed. It was observed that the frequency change, even in high frequencies, is almost insensible, making modal frequency based detection an inefficient damage detection scheme. Then wave propagation capabilities of the model have been investigated. Response of the model has first been verified by comparing with the results obtained from classical finite element model, followed by the demonstration of a wave propagation of a two-layer beam to investigate the how the wave propagation response reacts to different damage levels in the beam.

Finally, the developed SFEM has been applied to a SHM application by demonstrating the wave propagation response of a multi-layered beam structure. The wave propagation response of the multi-layered beam used has also been compared with a finite element model to show the effectiveness in damage detection of the model developed. The same model has also been used in a frequency sensitivity study to show the effect of different excitation frequencies on damage

detection. It was found that higher frequency excitation signal is more efficient in capturing the level of the damage located in the beam.

In summary, a multi-layered beam model was developed to characterize the wave propagation in for the identification and the assessment of a damage located on a multi-layered beam structure. The developed model can be used to conduct damage analysis for multi-layered beam structures.

There are several lines of research arising from this work. Future work includes implementing this method for a composite beam. In addition improvement of the model by implementing a full or several layer loss case to identify different types of damage for composite/multi-layered structures is another line of research. Experimental verification and validation is also an interest that should be pursued.

REFERENCE

[1] Giurgiutiu, V., *Structural Health Monitoring, Academic* Press, 2008.

[2] Reddy, J. N., *Mechanics of Laminated Composite Plates and Shells*, CRC Press, 2004.

[3] Krajcinovic, D., "Sandwich Beam Analysis", *Journal of Applied Mechanics*, Vol. 39, pp. 773-778.

[4] Zuo, Q.H. and Hjelmstad, K.D., "Piecewise Linear Warping Theory for Multilayered Elastic Beams", *Journal of Engineering Mechanics*, Vol. 124, No. 4, April 1998.

[5] Banerjee, J.R., 2003, "Free Vibration of Sandwich Beams Using The Dynamic Stiffness Method", *Computers & Structures*, Vol. 81, No. 18, pp. 1915-1922.

[6] Banerjee, J.R., and Sobey, A.J., 2005, "Dynamic Stiffness Formulation and Free Vibration Analysis of a Three-Layered Sandwich Beam", *International Journal of Solids and Structures*, Vol. 42, No. 8, pp. 2181-2197.

[7] Banerjee, J.R., Cheung, C.W., Morishima, R., Perera, M. and Njuguna, J., 2007, "Free Vibration of a Three-Layered Sandwich Beam Using Dynamic Stiffness Method and Experiment", *International Journal of Solids and Structures*, Vol. 44, pp. 7543-7563.

[8] Atlihan, G., Callioglu, H., Conkur, E.S., Topcu, M., "Free Vibration Analysis of the Laminated Composite Beams by Using DQM", *Journal of Reinforced Plastics and Composites*, Vol. 28, No. 07/2009, pp. 881-892.

[9] Lee, U., *Spectral Element Method in Structural Dynamics*, John Wiley & Sons (Asia) Ltd., Singapore, 2008.

[10] F. Moser, L. J. Jacobs, J. Qu, Modeling elastic wave propagation in waveguides with the finite element method, NDT &E International 32 (1999) 225-234.

[11] C. Yang, L. Ye, Z. Su, M. Bannister, Some aspects of numerical simulation for lam wave propagation in composite laminates, Composite Structures 75 (2006) 267-275.

[12] T. Kocaturk, A. Eskin, S. D. Akbas, Wave propagation in piecewise homogeneous cantilever beam under impact force, International Journal of the Physical Sciences 6 (2011) 3867-3874.

[13] Doyle, J.F., *Wave Propagation in Structures*, Second Edition, Springer-Verlag, 1997.

[14] D. Beskos, G. Narayanan, 1983, "Dynamic Response of Frameworks by Numerical Laplace Transform", *Computer Methods in Applied Mechanics and Engineering*, Vol. 37, pp.

289-307.
[15] Leung, A. Y. T., 1993, *Dynamic Stiffness and Substructures*, Springer Verlag, London.
[16] S. Gopalakrishnan, A. Chakraborty, D. R. Mahapatra, Spectral finite element method, Springer (2007).
[17] J. F. Doyle, A spectrally formulated finite element for longitudinal wave propagation, International Journal of Analytical and Experimental Modal Analysis 3 (1988) 1-5.
[18] J. F. Doyle, T. N. Farris, A spectrally formulated finite Element for flexural wave propagation in beams, International Journal of Analytical and Experimental Modal Analysis 5 (1990) 13-23
[19] S. Gopalakrishnan, M. Martin, J. F. Doyle, A matrix methodology for spectral analysis of wave propagation in multiple connected Timoshenko beams, Journal of Sound and Vibration 158 (1992) 11-24.
[20] F. Martin, S. Gopalakrishnan, J. F. Doyle, Wave propagation in multiply connected deep waveguides, Journal of Sound and Vibration 174 (1994) 521–538.
[21] D. R. Mahapatra, S. Gopalakrishnan, T. S. Shankar, Spectral-element-based solution for wave propagation analysis of multiply connected unsymmetric laminated composite beams, Journal of Sound and Vibration 237 (2000) 819–836.
[22] D. R. Mahapatra, S. Gopalakrishnan, A spectral finite element model for analysis of
axial-flexural-shear coupled wave propagation in laminated composite beams, Composite Structures 59 (2003) 67–88.
[23] R. Ruotolo, A spectral element for laminated composite beams: theory and application to pyroshock analysis, Journal of Sound and Vibration 270 (2004) 149-169.
[24] M. Palacz, M. Krawczuk, W. Ostachowicz, The spectral finite element model for analysis of flexural-shear coupled wave propagation: Part 1: Laminated multilayer composite beam, Composite Structures 68(2005) 37-44.
[25] M. Mitra, S. Gopalakrishnan, Wavelet based spectral finite element for analysis of coupled wave propagation in higher order composite beams, Composite Structures 73 (2006) 263-277.
[26] H. Peng, L. Ye, G. Meng, S. Mustapha, F. Li, Concise analysis of wave propagation using the spectral element method and identification of delamination in CF/EP

composite beams, Smart materials and structures 19 (2010) 1-11.
[27] U. Lee, I. Jang, Spectral element model for axially loaded bending-shear-torsion coupled composite Timoshenko beams, Composite Structures 92 (2010) 2860-2870.
[28] Krawczuk, M., Palacz, M., Ostachowicz, W., 2003, "The Dynamic Analysis of a Cracked Timoshenko Beam by the Spectral Element Method", *Journal of Sound and Vibration*, Vol. 264, pp. 1139-1153.
[29] S. Gopalakrishnan, A. Chakraborty, D.R. Mahapatra, "*Spectral Finite Element Method: Wave Propagation, Diagnostics and Control in Anisotropic and Inhomogeneous Structures*", Springer, Berlin, 2007.
[30] J. F. Doyle, A spectrally formulated finite element for longitudinal wave propagation, International Journal of Analytical and Experimental Modal Analysis 3 (1988) 1-5.
[31] J. F. Doyle, T. N. Farris, A spectrally formulated finite Element for flexural wave propagation in beams, International Journal of Analytical and Experimental Modal Analysis 5 (1990) 13-23.
[32] S. Gopalakrishnan, M. Martin, J. F. Doyle, A matrix methodology for spectral analysis of wave propagation in multiple connected Timoshenko beams, Journal of Sound and Vibration 158 (1992) 11-24.
[33] F. Martin, S. Gopalakrishnan, J. F. Doyle, Wave propagation in multiply connected deep waveguides, Journal of Sound and Vibration 174 (1994) 521–538.
[34] Lee, J., 1999, "Free Vibration Analysis of Delaminated Composite Beams", *Computers & Structures*, Vol. 74, pp. 121-129.
[35] Wang, G, Wereley, N.M., "Free Vibration Analysis of Rotating Blades with Uniform Tapers", *AIAA Journal*, Vol. 42, No. 12, December, 2005, pp. 2429-2437.
[36] Wang, G, Wereley, N.M., "Spectral Finite Element Analysis of Sandwich Beams with Passive Constrained Layer Damping", *ASME Journal of Vibration and Acoustics*, Vol. 124, No. 3, July, 2002, pp. 376-386.
[37] Krawczuk, M., Palacz, M., Ostachowicz, W., 2003, "The Dynamic Analysis of a Cracked Timoshenko Beam by the Spectral Element Method", *Journal of Sound and Vibration*, Vol. 264, pp. 1139-1153.